A new hybrid PSO-YUKI for double cracks identification in CFRP cantilever beam

A new hybrid PSO-YUKI for double crack identification in CFRP cantilever beam

Abdelwahhab Khatir[a], Roberto Capozucca[a], Samir Khatir*[b], Erica Magagnini[a], Brahim Benaissa[c], Cuong Le Thanh[b] and Magd Abdel Wahab[d]

a) Structural section DICEA, Polytechnic University of Marche, Ancona, Italy
a.khatir@pm.univpm.it; r.capozucca@staff.univpm.it; e.magagnini@univpm.it;
b) Faculty of Civil Engineering, Ho Chi Minh City Open University, Ho Chi Minh City, Vietnam.

c) Toyota Technological Institute, Department of Mechanical Systems Engineering, Design Engineering Lab, 468-8511 Aichi, Nagoya, Tempaku Ward, Hisakata, 2 Chome-12-1, Japan benaissa@toyota-ti.ac.jp;

d) Soete Laboratory, Faculty of Engineering and Architecture, Ghent University, Technologiepark Zwijnaarde 903, B-9052, Zwijnaarde, Belgium

Abstract: The durability and simplicity of the programming of meta-heuristic algorithms make them important in the optimization field. This paper presents a novel application for double crack identification in carbon fibers reinforced polymer (CFRP) cantilever beams based on experimental and numerical analysis using enhanced optimization techniques. A new hybrid algorithm Particle Swarm Optimization and YUKI (PSO-YUKI) is proposed and combined with Radial Basis Functions (RBF) for solving fast inverse problems. The direct problem is based on the results of the dynamic experimental test of CFRP laminate, measuring the dynamics characteristics of a healthy beam, and the variation in the response corresponding to different scenarios of double crack with different depths. The Finite Element Method (FEM) is provided to simulate this vibrational behavior considering double crack in different locations. The goal of creating a damage identification method that is both accurate and with high computational performance. The idea of building models based on the combination of vibrational responses issued from the experiment and simulation. The suggested method is tested based on collected data from numerical and experimental modal analysis in the case of undamaged and damaged CFRP laminate to demonstrate its accuracy and efficiency. The provided results show the robustness of PSO-YUKI compared with PSO for double crack depth identification.

Keywords: Double crack prediction, PSO, PSO-YUKI, Finite Element Analysis, Experimental modal analysis.

1. Introduction

Structural health monitoring (SHM) is extremely important for sustaining and preserving the service life of civil structures, it started with visual inspection and developed over time into Structural Damage Detection (SDD). Damage detection is the most critical component of SHM, which is defined as a method for identifying damage and assessing its severity. A review of the different applications of guided waves for SHM is presented in [1]. In order to make the monitoring process more practicable, a large number of approaches have been developed to identify, localize, and quantify structural damage [2-5].

In recent years, vibration-based damage detection approaches have received a lot of interest from the research community as a way to get around the constraints of traditional SHM methods. To identify damage in a structure, modal parameters, such as natural frequencies, mode shapes, transmissibility, and frequency response function (FRF) are commonly used [5]. In source [6] a speckle shear interferometric approach was used to measure the rotational field of statically loaded clamped-free and free-free aluminum beams. Transverse force and bending moment were calculated from these observations by successively differentiating a rotating field for a healthy structure and one with two cuts. The differences in these parameters for healthy and damaged structures were used to calculate damage indicators defined by rotation field, displacement, bending moment, and shear force. In [7], Capozucca performed a free vibration analysis on a cantilever CFRP beam that was damaged by considering two notches at the fixed end. Viglietti et al. [8] suggested a component-wise technique for analyzing the free vibration of tapered composites. This approach has also been used to investigate damaged aircraft structures and three-stringer spars [9, 10], and civil structures [11].

Various undetectable damages are often present in composit9e materials, such as cracks in fibers and matrix, and interfaces between fibers and matrix, leading to fatigue failures [12]. Many theoretical and experimental studies have been conducted on the issue of cracks in beams made of non-homogeneous materials [13-17]. It was developed a theoretical model that describes the behaviour of CFRP simply supported beams based on previous research on the free vibration of beams with single and multiple notches. There are many works in Ref. [18] based on cracks in composite materials or notched CFRP elements. A number of analytical methods have been developed to study the initiation and propagation of damage in composite elements [18-20]. Others have investigated the experimental behavior of damaged FRP elements in order to better understand and/or predict the failure of composite materials with cracks and/or notched CFRP elements [21].

Optimization algorithms have been employed by many researchers for damage detection, various optimization algorithms were created in an attempt to find approximate solutions to problems such as identifying structural damage, Arora and Singh [22] proposed the Butterfly Optimization Algorithm (BOA), and their solution to three engineering optimization problems involves an improved butterfly optimization algorithm using ten chaotic maps [23]. Particle Swarm Optimization (PSO) and Genetic Algorithms (GA) are optimization techniques that can be used to solve the structural damage identification problem. Researchers have used these and other optimization techniques to detect damage in different structures, including Particle Swarm Optimization (PSO) [24-29], Genetic Algorithms (GA) [30-32], Multi-objective Optimization (MO) [33, 34], Cuckoo Search Optimization (CS) [35, 36]. Research on damage detection in an Aluminum plate was given by Livani et al. [37]. To compute the horizontal boundary displacement at selected points, the extended Spectral Finite Element method (XSFEM) was employed with an enhanced particle swarm optimization (PSO) based on an active/inactive flaw strategy. Two types of damages were considered in this study. Two-dimensional coordinates of the tip characterized a crack, and two-dimensional coordinates of the center characterized a circular flaw. Moezi et al. [38] developed an improved CS method for detecting open-edge cracks in cantilever Euler-Bernoulli beams, where the crack was defined by its depth and position. The natural frequencies acquired from an experimental hammer test were then employed as the structural response in this investigation. Zhou et al [39] proposed structural identification using an improved butterfly optimization algorithm with an adaptive sampling test and search space reduction method. YUKI algorithm was suggested for the problem of damage identification based on elastic boundary displacement [40].

Researchers have used Artificial Neural Networks (ANN) to identify damage location and severity using various types of input and output variables since they are an efficient tool for pattern recognition. Recent structural health monitoring research has tended to use artificial intelligence techniques as well as ANN to analyze mechanical structure damages [41]. The most positive aspect of employing ANN is that it is capable of outstanding pattern recognition, auto-association, self-organization, self-learning, and nonlinear modeling. From inaccurate, unreliable, inconsistent, uncertain, and noise-polluted data, ANN is capable of retrieving precise and reliable information. As a result, ANN is fault tolerant, allowing for automated defect identification after the network has been properly trained [42]. Gomes et al [43] applied an optimized methodology based on GA and ANN for the delamination identification of CFRP laminated composite plates involving the use of reduced mode shapes and computational tools. ANN was also improved using optimization techniques like PSO [44] and Arithmetic Optimization Algorithm (AOA) [45] for several structural damage identification. Luo et al [46], proposed a laminated composite plate and turbine-bladed disk to illustrate the capability of the proposed hybrid enhanced Monte Carlo Simulation (HEMCS) for approximation of failure probability. In their methodology, they have based on reliability-based multidisciplinary design optimization (RBMDO)[47-50].

Through a study of a common benchmark, this work discusses a new combined approach based on PSO and YUKI Algorithm using Radial Basis Function (RBF) for structural damage assessment, emphasizing the need for a good definition of the error function that analyzes the differences between experimental data and FE model results. This paper investigates the use of a novel hybrid algorithm PSO-YUKI to determine crack depth in a cracked CFRP cantilever laminate by minimizing the cost function and comparing it to PSO alone through numerical and experimental tests to verify its accuracy.

2. PSO-YUKI

The Particle Swarm Optimization algorithm (PSO) is one of the most important optimization methods, and the earliest naturally inspired optimization algorithm [51], its search technique assumes that the solutions move in the design space, with a variable velocity. There exist several solutions simultaneously, called population, where the position of each solution, also called a particle, is decided

based on two reference points. Considering that in each iteration, the solutions are evaluated according to the objective function, the first point is called the global best, which is simply the position inside the design space that corresponds to the best objective function value. If a better position is found in the next iteration, then the new point is dubbed Global best X_{best}, so the position of this point is variable and represents the progress of the search. The second reference point is called the personal best X^i_{best}, which is similar to the first reference point, but as stated in the name, it tracks the search progress of each individual solution, so in the case of a population equal to 10, there exist 10 personal best points, one for each solution. Each particle in PSO moves in the design space with a variable velocity, based on an equation that has three main components. First, the inertia motivates the particles to move in the same direction. Second, is the individual part, where each particle moves toward its personal best position. And the last part is social, where all the particles go toward the global best. The combination of these three heuristics creates a very complex behavior. The solutions will efficiently search the design space because the position of the reference point changes according to the new results. Initially, the change is drastic, which encourages exploration behavior, but with progress, the change in the reference points is less drastic, thus encouraging exploitation, in which the solution is finding the variables representing the fine details. The Equation guiding this behavior is as follows:

$$V^i_{new} = wV^i_{old} + c_1 r_1\left(X^i_{best} - X^i_{old}\right) + c_2 r_2\left(X_{best} - X^i_{new}\right) \quad (1)$$

$$X^i_{new} = X^i_{old} + V^i_{new} \quad (2)$$

Where X^i_{new} denotes the position at the current iteration of particle$i$ and X^i_{old} is the position at the previous iteration. The same for velocity V^i_{new} and V^i_{old} . w is the weight parameter, c_1 *and* c_2 are search parameters, set equal to 2 here. And, $r_1 and\ r_2$ are two different random values between 0 and 1.

YUKI algorithm on the other hand is a newly suggested algorithm that uses the principle of dynamic search space reduction [40], this algorithm is not inspired by nature. It is based on the ideas of exploration and exploitation of search algorithms, it suggests a simple formulation for creating a local search area inside the design space. Where the size of this focus zone is defined by the distance D, expressed in equation 3, as the difference, in all dimensions, between the position called MeanBest and the position of the global best. Where MeanBest is the centre of the historical best points cloud. The distance D changes according to the search results and tends to get smaller throughout the progress of the search thus focusing the search algorithm in a smaller area. The position of the local search area is guided by the position of the global best point, according to equations 2 to 3 which define the boundaries of this focus area in each dimension. LT and LB are respectively the local top and bottom boundaries of the local search space.

$$D = |X_{best} - X_{MeanBest}| \quad (3)$$

$$LT = X_{best} + D \quad (4)$$

$$LB = X_{best} - D \quad (5)$$

Besides the search space reduction idea, this algorithm generates in each iteration, random points X^i_{loc} inside this focus area. The search performance is then based on two behaviors. First, the exploration, where the generated solutions are created outside the local search area, in the direction of their personal best points, guided by equation 6 and 7, where E^i is the reach distance for exploration.

$$E^i = X^i_{loc} - X^i_{best} \quad (6)$$

$$X^i_{new} = X^i_{loc} + E^i \quad (7)$$

The second behavior is exploitation where multiple solutions are created around the global best. F^i is the search distance for exploration expressed by equation 8. and equation 9 helps find better solutions ions through randomness. where $rand$ here is the random value between 0 and 1.

$$F^i = X^i_{loc} - X_{best} \tag{8}$$

$$X^i_{new} = X^i_{loc} - rand \times F^i \tag{9}$$

The two behaviors of exploration and exploitation are performed simultaneously in YUKI algorithm, by dedicating two parts of the population to each task. The suggested hybrid algorithm intends to improve the search behaviour of PSO algorithm by introducing the simultaneous exploration-exploitation behavior of YUKI algorithm. This is done by calculating the E^i distance according to the distance from the personal best and to the global best according to equation 10. The combined heuristics results in complex search behaviour that allows the PSO algorithm to spend less effort on exploring various regions by individual solutions, but use the whole population effort in a synchronized manner. The proposed algorithm framework diagram is resented in **Figure 1**.

$$E^i = wV^i_{old} + c_1 r_1\left(X^i_{best} - X^i_{old}\right) + c_2 r_2\left(X_{best} - X^i_{new}\right) \tag{10}$$

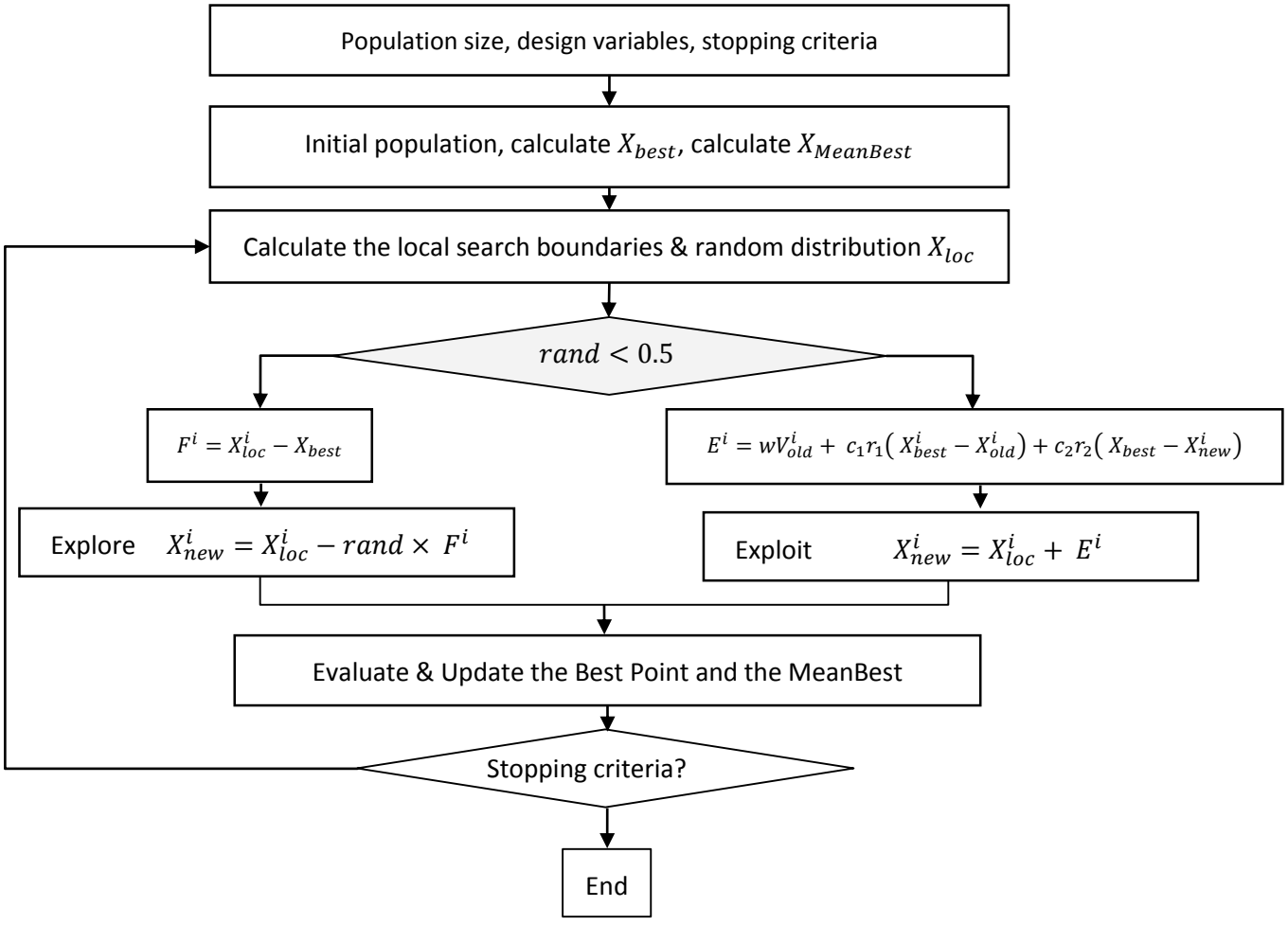

Figure 1. PSO- YUKI Algorithm framework diagram.

3. Inverse identification

The Radial Basis Functions (RBF) are a very efficient method for interpolation between existing data [52, 53]. It creates an approximation for a function $f(x)$, based on a set of N nodes x_i, in which the values of the function are known. Using a combination of g_i functions. The basis functions g_i of the Euclidian distance is employed in this paper.

$$f(x) \approx \sum_{i=1}^{N} \alpha_i g_i(x) \tag{11}$$

$$g_i(x) = g_i(\|x - x_i\|), i = 1, 2, \dots, N \tag{12}$$

To calculate the coefficients α_i, it considers that the interpolation is exact in all N nodes, thus the system of N equations defined by Eq 12, where y_j are the values of the function in the known nodes. The G matrix is then calculated once according to equation 13, and the approximation is written in equation 14 to calculate the interpolation coefficients α_i. Once this is achieved, the approximation function can be performed at any given point inside the range of the initial set of points x_i [52].

$$f(x_j) = y_j = \sum_{i=1}^{N} \alpha_i g_i(x_j), j = 1, \dots, N \tag{13}$$

$$G = [g_1(x_1) \ \dots \ g_N(x_1) \ \vdots \ddots \vdots \ g_1(x_N) \ \dots \ g_N(x_N)]; \ \ \alpha = [\alpha_1, \alpha_2, \dots, \alpha_N]^T; \ \ Y = [y_1, y_2, \dots, y_N]^T \tag{14}$$

$$\alpha \cdot G = Y \tag{15}$$

ANN on the other hand is a widely known method. In this method, the systems information is stored in the weights of the network nodes. So in order for the network to approximate the function $f(x)$, these weights are optimized in a process called training. During this, a smaller set of data, called the validation dataset, is used to test the quality of the network predictions. An optimization algorithm is used to search for the values of the optimal weights that correspond to the highest precision [54]. In this paper, we build a model that represents the vibrational characteristics of the damaged and the undamaged beams, using the results issued from the experiment plus data issued from the FEM simulation. Both RBF and ANN models are then employed for the inverse identification of damages.

The suggested algorithm of YUKI-PSO will search for the damage parameters that correspond to the optimal structural response, according to the following objective function, with P representing the damage parameters:

$$f^i(P) = \frac{\|u^i(p_0) - u^i(p)\|^2}{\|u^i(p_0)\|^2} \text{ with } i = 1, 2, 3. \tag{16}$$

$$F_1(P_{opt}) = \min(f^1(P), f^2(P), f^3(P)) \tag{17}$$

$$F_2(P_{opt}) = \text{Mean}(f^1(P), f^2(P), f^3(P)) \tag{18}$$

$$f(P) = F_1 + F_2 \tag{19}$$

This is designed to isolate the noisy effect created by the combination of all vibrational modes together. And identify the damages based on the possibility of fit between all vibrational modes, but also in case there is a fit in one or two modes only. F_1 calculates the minimum difference between the estimated response and reference response, obtained in one of the three modes. And F_2 calculates the average of these differences. The objective function is then the sum of F_1 and F_2.

4. Numerical experiments of PSO-YUKI

The performance of the suggested YUKI-PSO algorithm is examined in this section, using the classical benchmark functions utilized by most optimization researchers, detailed in the CEC reports [55]. The

functions presented here are divided into four sections: 1. Unimodal, 2. multimodal, 3. fixed-dimension unimodal, and 4. fixed-dimension multimodal. With 10 functions in each section.

The functions for this test are presented in **Tables 1 to 4**. Showing the equations, the function name, along with the global boundary of the search space and the dimensions of the problem. In **Table 1**. The selected unimodal functions for all functions. The size of design variables i.e. dimensions, is 30. **Table 2** shows the selected multimodal functions. Here also the size of design variables is 30 for all functions. **Table 3** shows the selected fixed dimensions unimodal functions. **Table 4** shows the selected fixed dimensions multimodal functions for this test. **Figure 2** shows the shape of some selected functions. The investigation results are obtained over 30 independent runs for each function, see **Figure 2**. Made with a population size of 30 and a maximum number of iterations of 200.

Table 1. Unimodal benchmark functions

$f_1(\mathrm{x}) = f(x_1, x_2, \ldots, x_n) = \sum_{i=1}^{n} x_i^2$	Sphere	[-5.12 5.12]	30
$f_2(\mathrm{x}) = f(x_1, \ldots, x_n) = \sum_{i=1}^{n} i x_i^2$	Powell Sum	[-1 1]	30
$f_3(\mathrm{x}) = x_1 + d(\sum_{i=2}^{n} x_i^2)^{\alpha}$	Powell Sum	[-5 5]	30
$f_4(x) = \sum_{i=1}^{29} (x_i^2)^{(x_{i+1}^2+1)} + (x_{i+1}^2)^{(x_i^2+1)}$	Brown	[-4 4]	30
$f_5(\mathrm{x}) = f(x_1, \ldots, x_{30}) = -exp(-0.5 \sum_{i=1}^{30} x_i^2)$	Exponential	[-2 2]	30
$f_6(x) = f(x_1, \ldots, x_{30}) = exp(-\sum_{i=1}^{30} (x_i/15)^{10}) - 2exp\left(-\sum_{i=1}^{30} x_i^2\right) \prod_{i=1}^{30} cos^2(x_i)$	Xin-She Yang N. 3	[-10 10]	30
$f_7(x) = f_7(x_1, \ldots, x_{30}) = \sum_{i=1}^{30} x_i^2 + (\sum_{i=1}^{30} 0.5 i x_i)^2 + (\sum_{i=1}^{30} 0.5 i x_i)^4$	Zakharov	[-10 10]	30
$f_8(x) = f(x_1, \ldots, x_{30}) = \sum_{i=1}^{30} \lvert x_i \rvert$	Schwefel 2.20	[-100 100]	30
$f_9(x) = f(x_1, \ldots, x_{30}) = \max_{i=1,\ldots,30} \lvert x_i \rvert$	Schwefel 2.21	[-100 100]	30
$f_{10}(x) = f(x_1, \ldots, x_{30}) = \sum_{i=1}^{30} \lvert x_i \rvert + \prod_{i=1}^{30} \lvert x_i \rvert$	Schwefel 2.22	[-10 10]	30

Table 2. Multimodal benchmark functions

$f_{11}(x) = f_{11}(x_1, \ldots, x_{30}) = \sum_{i=1}^{29} [100(x_{i+1} - x_i^2)^2 + (x_i - 1)^2]$	Rosenbrock	[-30 30]	30
$f_{12}(x) = f_{12}(x_1, x_2, \ldots, x_{30}) = \sum_{i=1}^{30} -x_i sin(\sqrt{\lvert x_i \rvert})$	Schwefel	[-500 500]	30
$f_{13}(x) = f_{13}(x_1, x_2, \ldots, x_{30}) = \sum_{i=1}^{30} [x_i^2 - 10cos(2\pi x_i) + 10]$	Rastrigin	[-5.12 5.12]	30
$\boldsymbol{f_{14}(x) = f(x_1, \ldots, x_{30}) = (\sum_{i=1}^{30} \lvert x_i \rvert) exp(-\sum_{i=1}^{30} sin(x_i^2))}$	Xin-She Yang N. 2	[-6.28 6.28]	30
$f_{15}(x) = f(x_1, \ldots, x_{30}) = (\sum_{i=1}^{30} sin^2(x_i) - e^{-\sum_{i=1}^{30} x_i^2}) e^{-\sum_{i=1}^{30} sin^2 \sqrt{\lvert x_i \rvert}}$	Xin-She Yang N. 4	[-10 10]	30
$f_{16}(x) = [(\lVert \mathrm{x} \rVert^2 - 30)^2]^{\alpha} + \frac{1}{n}(\frac{1}{2}\lVert \mathrm{x} \rVert^2 + \sum_{i=1}^{30} x_i) + \frac{1}{2}$	Happy Cat	[-2 2]	30
$f_{17}(x) = f(x_1 \ldots x_{30}) = 1 + \sum_{i=1}^{30} sin^2(x_i) - 0.1e^{(\sum_{i=1}^{30} x_i^2)}$	Periodic	[-10 10]	30
$f_{18}(x) = f(x_1, \ldots, x_{30}) = \sum_{i=1}^{30} i x_i^4 + \mathrm{random}[0,1]$	Quartic	[-1.28 1.28]	30
$f_{19}(x) = f(x_1, \ldots, x_{30}) = \sum_{i=1}^{30} \sum_{j=1}^{5} j sin((j+1)x_i + j)$	Shubert 3	[-10 10]	30

$f_{20}(x) = f(x_1, \dots, x_{30}) = 1 - cos(2\pi\sqrt{\sum_{i=1}^{D} x_i^2}) + 0.1\sqrt{\sum_{i=1}^{D} x_i^2}$	Salomon	[-4 4]	30

Table 3. Fixed dimensions unimodal benchmark functions

$f_{21}(x,y) = 2x^2 - 1.05x^4 + \frac{x^6}{6} + xy + y^2$	Three-Hump Camel	[-2 2]	2
$f_{22}(x,y) = -\frac{1+cos(12\sqrt{x^2+y^2})}{(0.5(x^2+y^2)+2)}$	Drop-Wave	[-5 5]	2
$f_{23}(x,y) = 100(y-x^3)^2 + (1-x)^2$	Leon	[-2 2]	2
$f_{24}(x,y) = (x+2y-7)^2 + (2x+y-5)^2$	Booth	[-10 10]	2
$f_{25}(x,y) = 0.26(x^2+y^2) - 0.48xy$	Matyas	[-10 10]	2
$f_{26}(x,y) = (x+10)^2 + (y+10)^2 + e^{-x^2-y^2}$	Brent	[-20 0]	2
$f_{27}(x,y) = 0.5 + \frac{sin^2(x^2+y^2)^2 - 0.5}{(1+0.001(x^2+y^2))^2}$	Schaffer N. 1	[-50 50]	2
$f_{28}(x,y) = -200e^{-0.2\sqrt{x^2+y^2}}$	Ackley N. 2	[-30 30]	2
$f_{29}(x,y) = x^2 + 2y^2 - 0.3cos(3\pi x) - 0.4cos(4\pi y) + 0.7$	Bohachevskyn N. 1	[-100 100]	2
$f_{30}(x,y) = 0.5 + \frac{cos^2(sin(\lvert x^2-y^2\rvert))-0.5}{(1+0.001(x^2+y^2))^2}$	Schaffer N. 4	[-100 100]	2

Table 4. Fixed dimensions multimodal benchmark functions

$f_{31}(x,y) = -\frac{sin^2(x-y)sin^2(x+y)}{\sqrt{x^2+y^2}}$	Keane	[-10 10]	2
$f_{32}(x,y) = sin^2(3\pi x) + (x-1)^2(1+sin^2(3\pi y)) + (y-1)^2(1+sin^2(2\pi y))$	Levi N. 13	[-10 10]	2
$f_{33}(x,y) = 100\sqrt{\lvert y-0.01x^2\rvert} + 0.01\lvert x+10\rvert$	Bukin N. 6	[-15 5]	2
$f_{34}(x,y) = -\lvert sin(x)cos(y)exp(\lvert 1 - \frac{\sqrt{x^2+y^2}}{\pi}\rvert)\rvert$	Holder-Table	[-10 10]	2
$f_{35}(x,y) = -0.0001(\lvert sin(x)sin(y)exp(\lvert 100 - \frac{\sqrt{x^2+y^2}}{\pi}\rvert)\rvert + 1)^{0.1}$	Cross-in-Tray	[-10 10]	2
$f_{36}(x,y,z) = \frac{4}{3}(x^2+y^2-xy)^{0.75} + z$	Wolfe	[0 2]	2
$f_{37}(x,y) = x^2 + y^2 + 25(sin^2(x) + sin^2(y))$	Egg Crate	[-20 20]	2
$\boldsymbol{f_{38}(x,y) = sin(x+y) + (x-y)^2 - 1.5x + 2.5y + 1}$	McCormick	[-1.5 4]	2
$f_{39}(x,y) = 10^5x^2 + y^2 - (x^2+y^2)^2 + 10^{-5}(x^2+y^2)^4$	Deckkers-Aarts	[-20 20]	2
$f_{40}(x,y) = \lvert x^2+y^2+xy\rvert + \lvert sin(x)\rvert + \lvert cos(y)\rvert$	Bartels Conn	[-500 500]	2

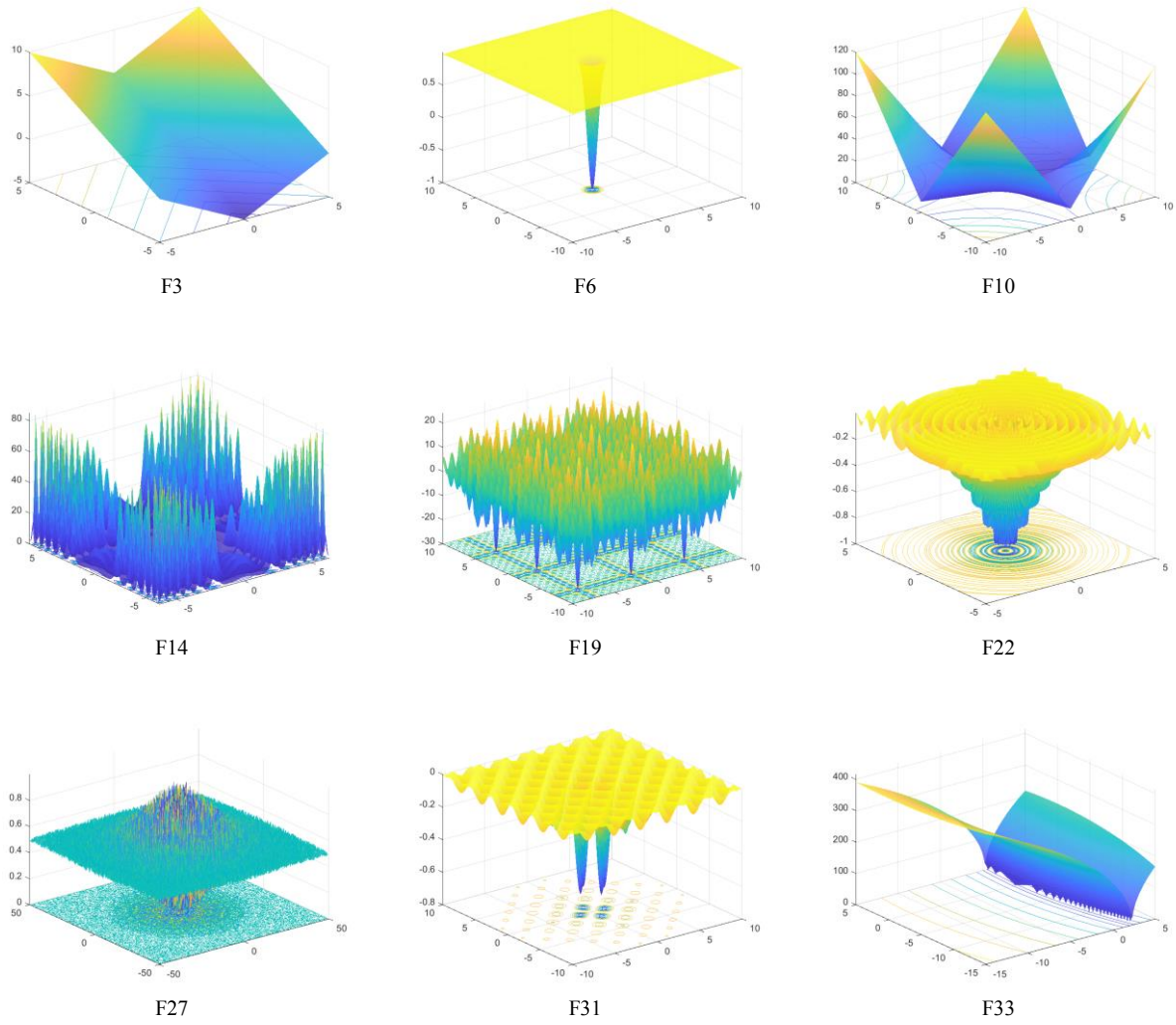

Figure 2. Shapes of some selected functions

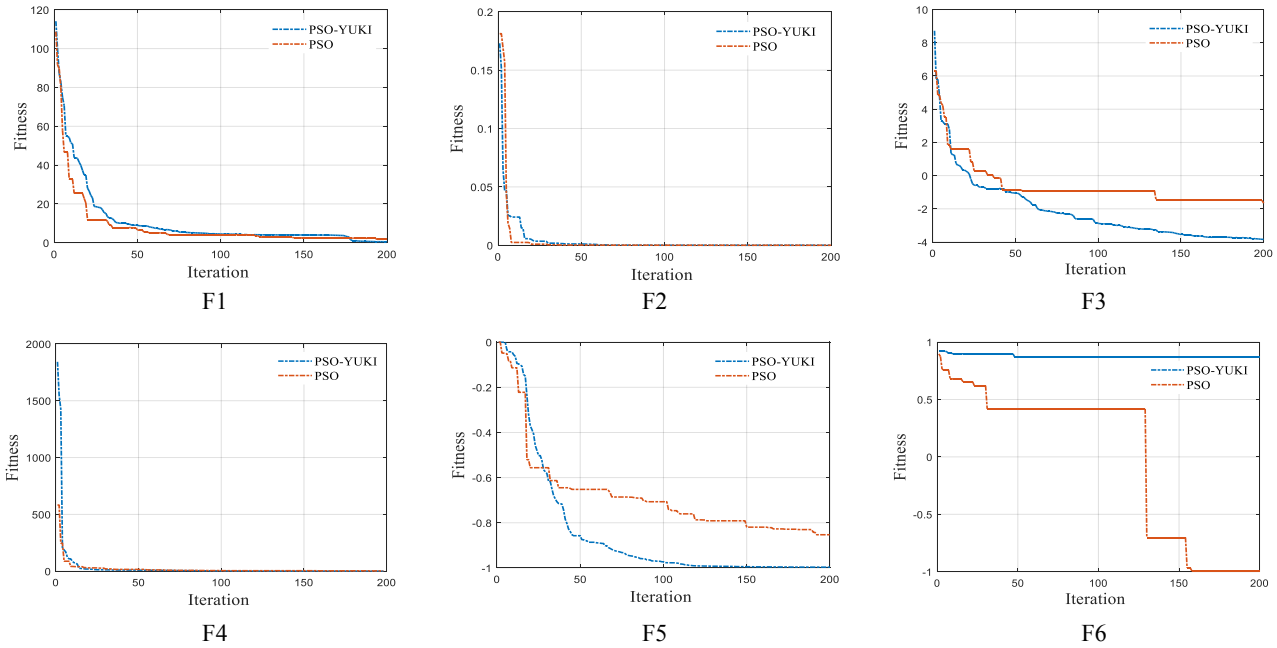

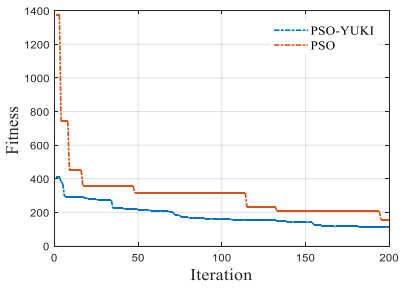

F7

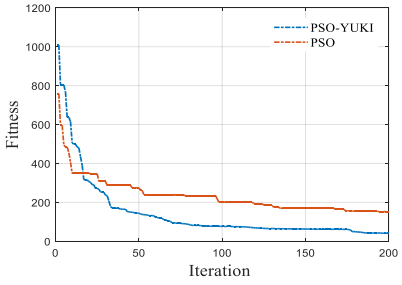

F8

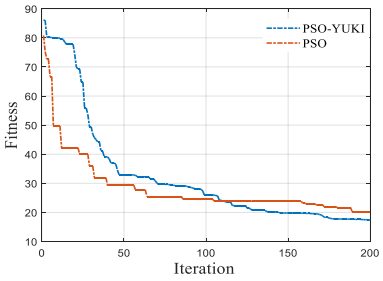

F9

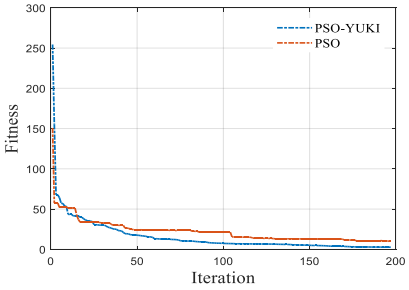

F10

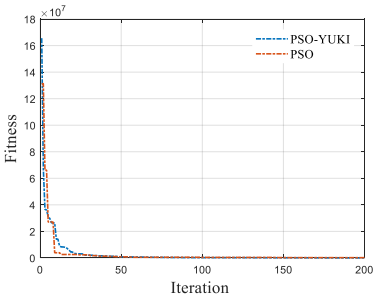

F11

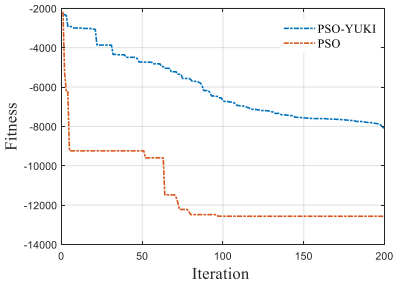

F12

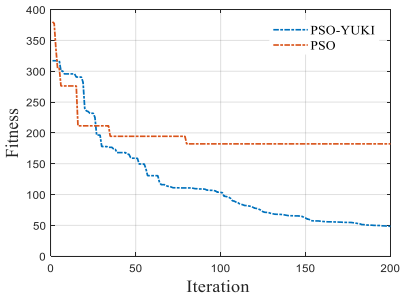

F13

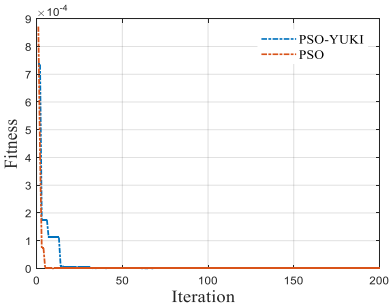

F14

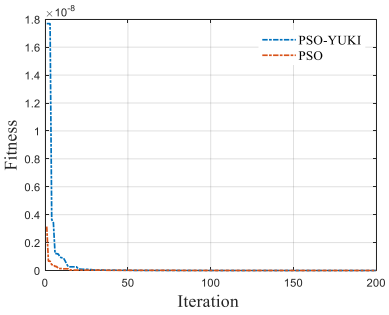

F15

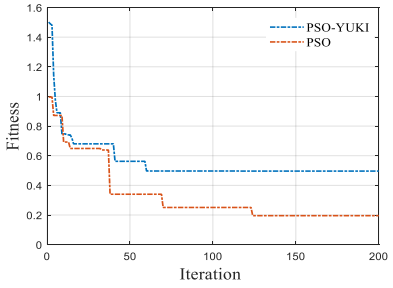

F16

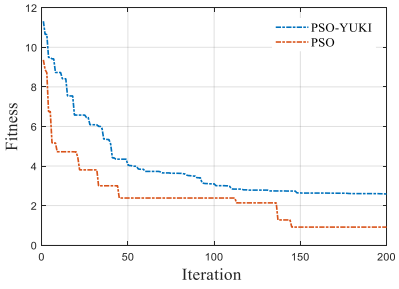

F17

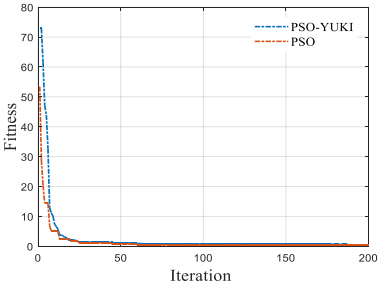

F18

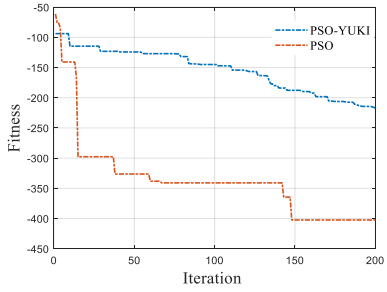

F19

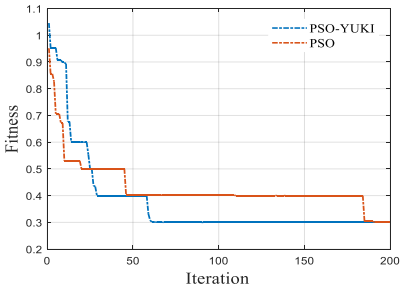

F20

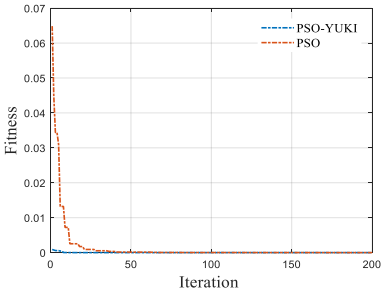

F21

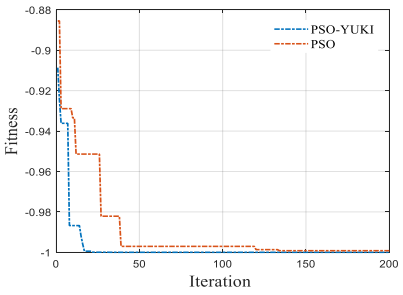

F22

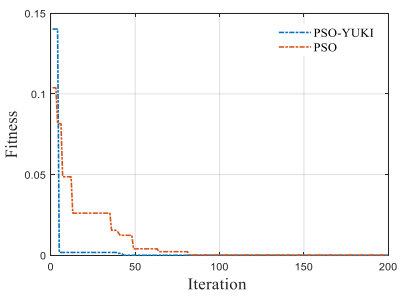

F23

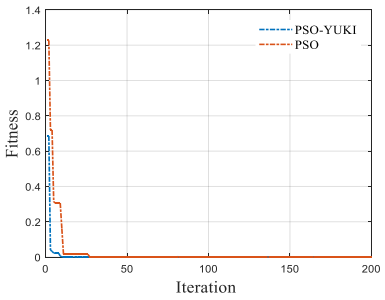

F24

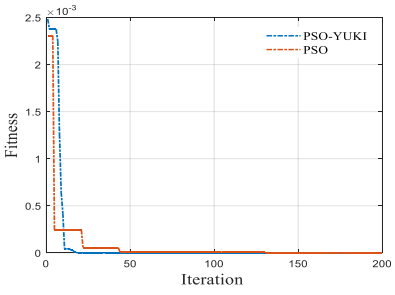

F25

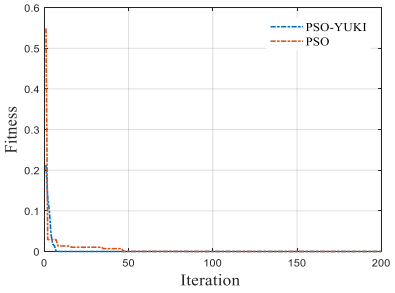

F26

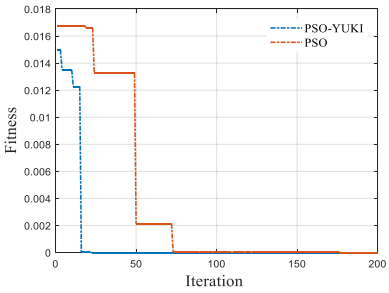

F27

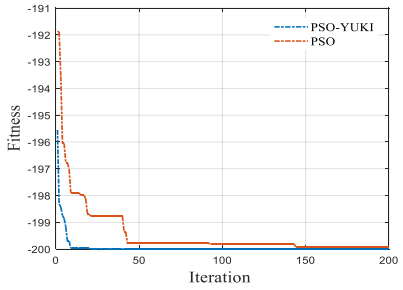

F28

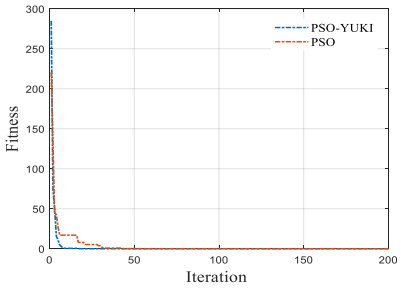

F29

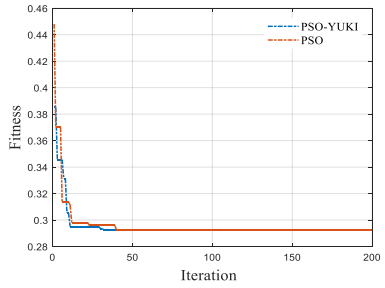

F30

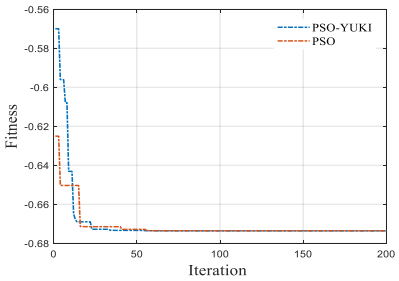

F31

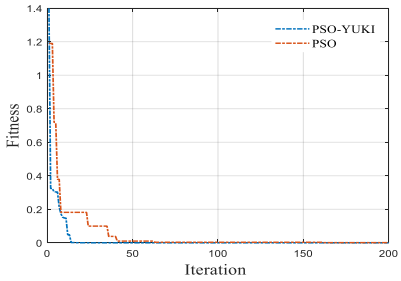

F32

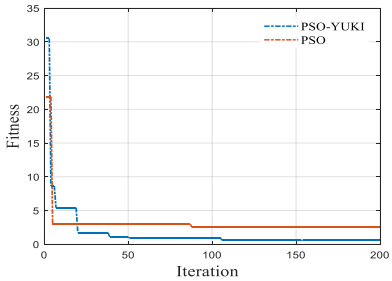

F33

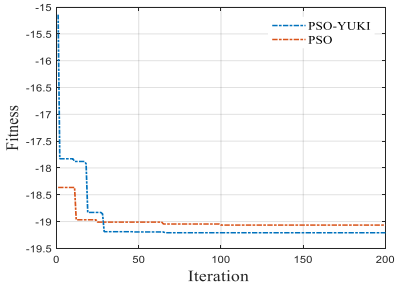

F34

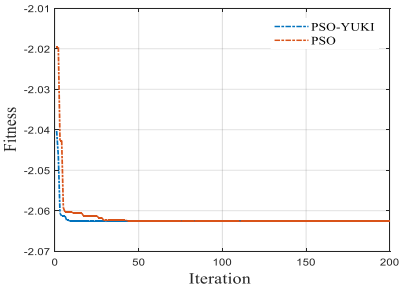

F35

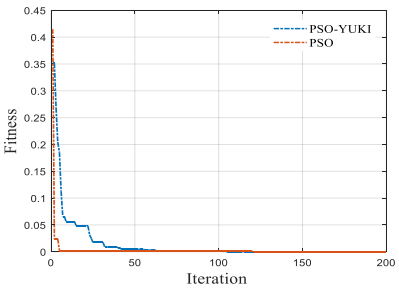

F36

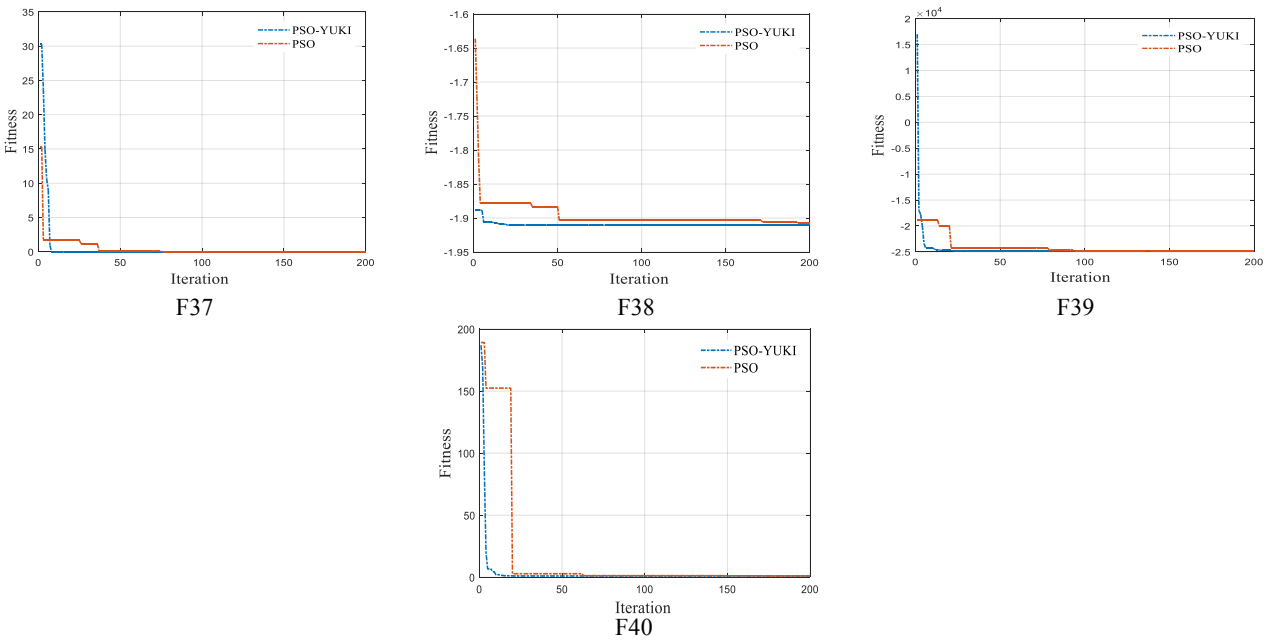

Figure 3. Convergence analysis of PSO and PSO-YUKI

According to the results of **Figure 3**, PSO-YUKI is able to provide very competitive results compared to PSO in most functions. However, the advantages of the suggested algorithm are more appearent in the heavily multimodal functions, such as benchmark functions 12, 16, 17 and 19. Where the objective function domain has a large number of local minima. This is most likely due to the focus ability of the YUKI algorithm, which helps avoid negative computational efforts where the best personal best positions are distributed across the search field, which prevents the quick advance of the search in PSO algorithm, but in the PSO-YUKI combination, the search is more forced to focus on the area around the global optimum. On the other hand, this focused search feature did not affect the search performance in unimodal function, where we can observe good performance. This is due to the flexibility of the focus feature in the YUKI algorithm, as it can expand to include neighboring areas and in different dimentions independently.

5. Application in structural health monitoring using PSO-YUKI

In this section vibration-based, inverse structural damage identification is analyzed. As mentioned in the literature, modal characteristics of structures such as mode shape and natural frequencies can be used as tools to detect the damaged zone in the structure. The CFRP cantilever beam model with its geometrical and mechanical properties presented in Table 5, is modeled using ABAQUS 16.4 Software. Cracks of various depths have been produced in several points along the beam's length.

Length L (mm)	Width W (mm)	Thickness t (mm)	Density ρ (kg/m^3)	Young modulus E (GPa)
300	21	5	1950	94

Table 5. Geometrical and mechanical characteristics of beam model

In order to test the accuracy of a novel algorithm PSO-YUKI combined with RBF for double crack depth prediction, three damage cases have been considered, in the first case (D_1), double crack was formed across the beam's clamped side width by increasing the crack depth from 0.25 mm to 15 mm with a 0.25 mm step. In the second case (D_2), four cracks were formed on the beam's clamped side and beam center's width by increasing the crack depth from 0.25 mm to 15 mm with a 0.25 mm step. In the third case (D_3), six cracks were formed on the beam's clamped side, center's width, and free side by increasing the crack depth from 0.25 mm to 15 mm with a 0.25 mm step, see Figure 3. Strike hammer position (S_{hp}) and accelerometer position are presented in **Figure 4**.

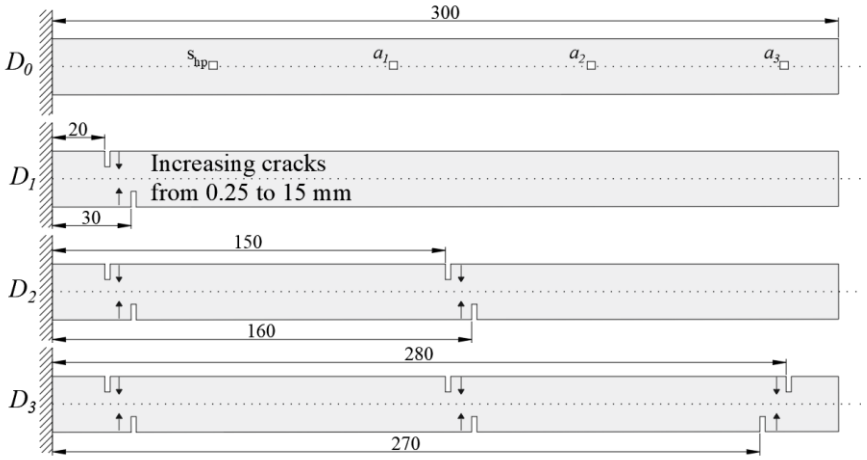

Figure 4. Considered CFRP beam model and damage cases

An experimental dynamic test was conducted on CFRP laminate specimens with mechanical characteristics listed in **Table 5** using a particular impact hammer to activate the structural component and accelerometers to calculate device acceleration. The LAN-XI TYPE 3050 - Brüel & Kjaer data acquisition system was used to investigate the dynamic behavior of the CFRP laminates. A piezoelectric accelerometer and impact hammer were connected to the data collection system using the input channels, respectively, as shown in **Figure 5**. Whereas a piezoelectric accelerometer (Type 4508) was inserted at regular 70 mm intervals on points a_1, a_2, and a_3 as shown in **Figure 5**. A measuring system capable of extracting frequency values by converted signals in the frequency domain using the Fast Fourier Transform (FFT) technique and Pulse software was used to make a set of 10 hits (h) for each location of the accelerometer a_i, and the average value was obtained.

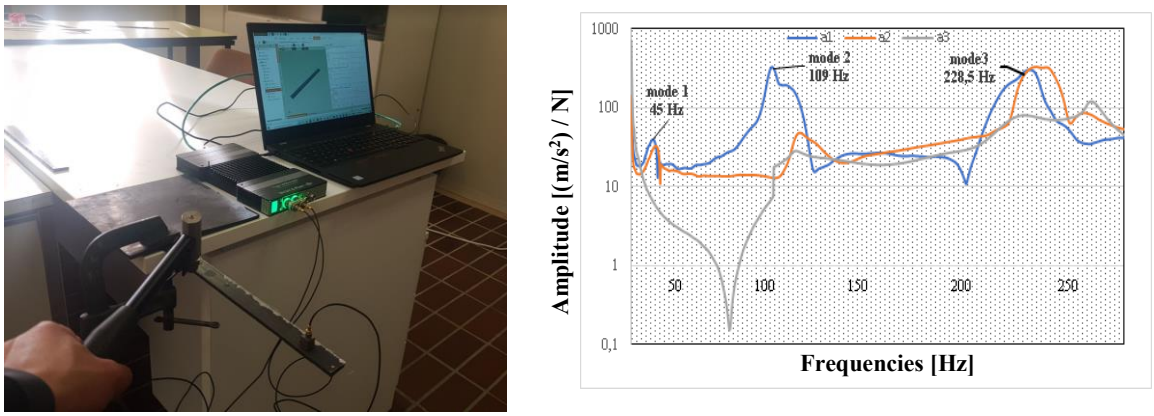

a *b*

Figure 5. Experimental set-up of healthy cantilever CFRP beam (*a*), FRF (*b*)

Table 6 shows the frequencies for undamaged (D_0) beam based on numerical and experimental studies. The torsional modes have been ignored for experimental reasons. The three first mode shapes of undamaged beam are presented in **Figure 6**.

Modes	FEM (Hz)	Experimental (Hz)
1	40.67	45.00
2	113.75	109.00
3	222.50	228.50

Table 6. Measured Frequencies of undamaged beam model

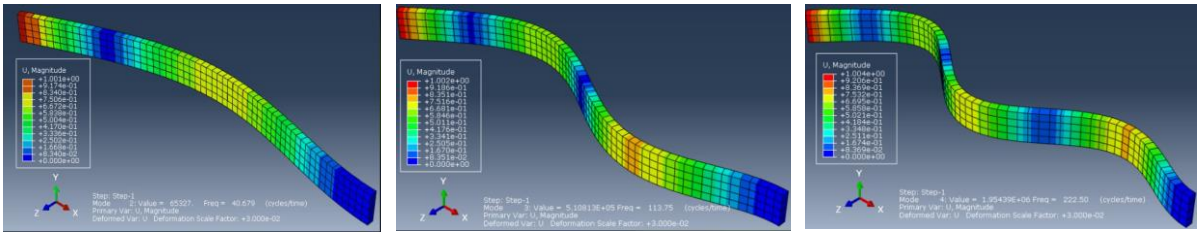

Mode 1 *Mode 2* *Mode 3*

Figure 6. The three first mode shapes of undamaged beam

6. Results and discussion

Inverse analysis using PSO-YUKI based on RBF is tested using three cases and compared with the original PSO. The datasets were collected from improved numerical simulation based on the analyzed results of damage cases (D_1, D_2, and D_3) to predict the crack depth. The double cracks depth predicted for each case are presented in Table 7.

Damage case	**D_1, D_2 and D_3**			
Crack depth (mm)	4	7	11	15

Table 7. Considered cracks depths

6.1. Damage case D_1

PSO and PSO-YUKI combined with RBF are tested in first damage case to predict clamped side double crack depth. The results for both algorithms to predict double crack depth are presented in **Figure 7**.

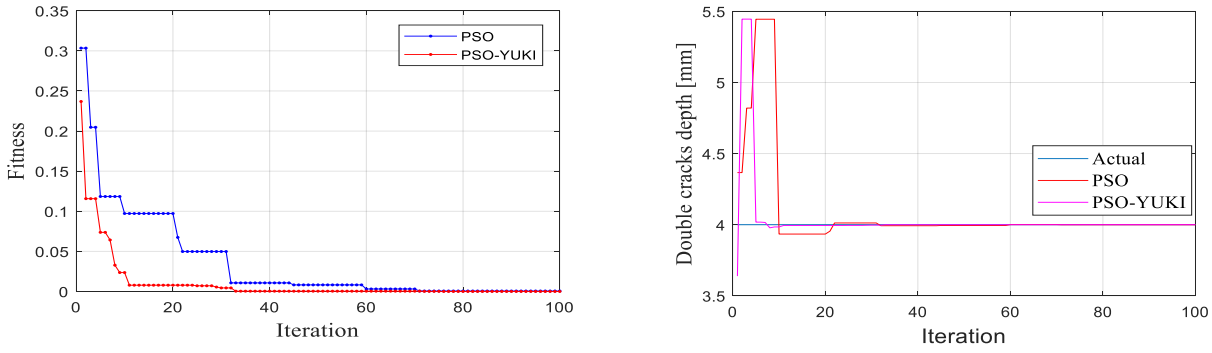

Test 1

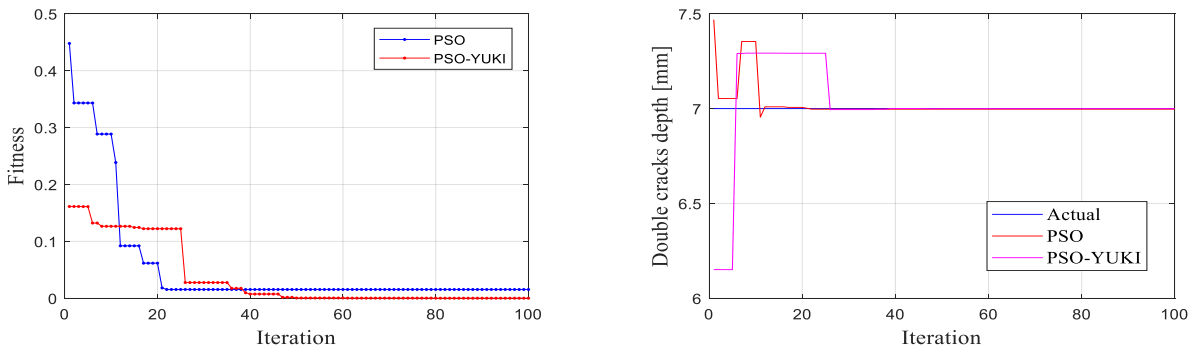

Test 2

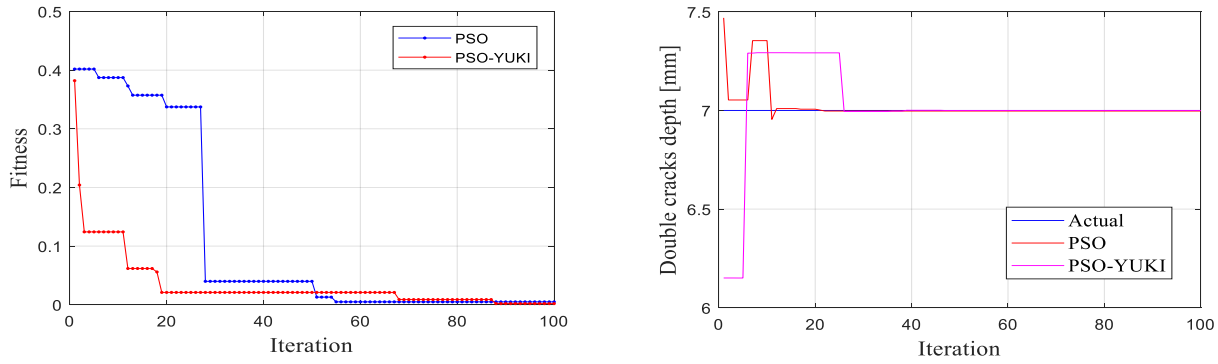

Test 3

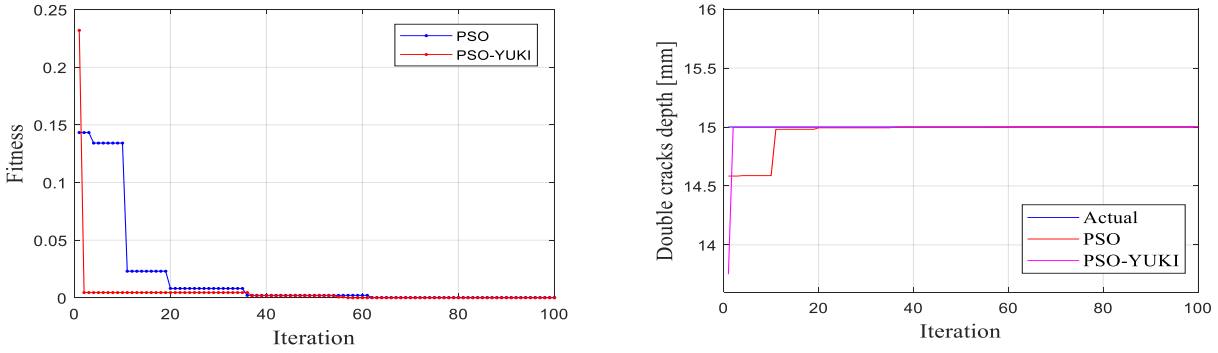

Test 4

Figure 7. PSO and PSO-YUKI performance for damage case D_1, predicting double cracks depth for 4 mm, 7 mm, 11 mm, and 15 mm.

The provided results for the first case show the robustness of PSO-YUKI compared to PSO combined to RBF in all tests with different double crack depth. The fitness and estimated double cracks depth values in 1, 15, 30, 50, 70, 85, and 100 iterations are presented in Table 8.

Crack depth	Optimization techniques	Number of iteration	Fitness	Estimated crack depth
4	PSO	1	0.30340	4.36620
	YUKI-PSO		0.23687	3.63863
	PSO	15	0.09720	3.93410
	YUKI-PSO		0.00782	3.99476
	PSO	30	0.04980	4.01220
	YUKI-PSO		0.00442	3.99704
	PSO	50	0.00820	3.99450
	YUKI-PSO		0.00036	3.99976
	PSO	70	0.00310	4.00080
	YUKI-PSO		0.00036	3.99976
	PSO	85	0.00059	3.99960
	YUKI-PSO		0.00001	3.99999
	PSO	100	0.00059	3.99960
	YUKI-PSO		0.00000	4.00000
7	PSO	1	0.44791	7.46920
	YUKI-PSO		0.16126	6.15099
	PSO	15	0.09214	7.00950
	YUKI-PSO		0.12443	7.29225
	PSO	30	0.01542	6.99709
	YUKI-PSO		0.02759	6.99479
	PSO	50	0.01542	6.99709
	YUKI-PSO		0.00044	6.99992
	PSO	70	0.01542	6.99709
	YUKI-PSO		0.00022	6.99996
	PSO	85	0.01542	6.99709
	YUKI-PSO		0.00006	6.99999
	PSO	100	0.01542	6.99709

	YUKI-PSO		0.00005	6.99999
11	PSO	1	0.40188	6.03154
	YUKI-PSO		0.38210	8.65327
	PSO	15	0.35732	6.02146
	YUKI-PSO		0.06180	10.98778
	PSO	30	0.03991	11.01461
	YUKI-PSO		0.02102	11.00770
	PSO	50	0.03991	11.01461
	YUKI-PSO		0.02102	11.00770
	PSO	70	0.00493	11.00181
	YUKI-PSO		0.00887	11.00325
	PSO	85	0.00493	11.00181
	YUKI-PSO		0.00887	11.00325
	PSO	100	0.00493	11.00181
	YUKI-PSO		0.00196	11.00072
15	PSO	1	0.14337	14.58388
	YUKI-PSO		0.23200	13.75158
	PSO	15	0.02308	14.98068
	YUKI-PSO		0.00458	14.99614
	PSO	30	0.00814	14.99315
	YUKI-PSO		0.00458	14.99614
	PSO	50	0.00216	14.99818
	YUKI-PSO		0.00188	14.99841
	PSO	70	0.00027	14.99978
	YUKI-PSO		0.00005	14.99996
	PSO	85	0.00027	14.99978
	YUKI-PSO		0.00005	14.99996
	PSO	100	0.00027	14.99978
	YUKI-PSO		0.00004	14.99997

Table 8. Fitness and estimated double cracks depth values of damage case D_1 in 1, 15, 30, 50, 70, 85, and 100 iterations

As seen in Table 8, the best results are boldfaced that are mostly provided by PSO-YUKI based on estimated crack depth and fitness. As opposed to the benchmark functions where the search performances were competitive, in the problem of crack identification, the suggested algorithm is clearly advantageous. The seed of convergence is significantly higher with PSO-YUKI algorithm. under the stopping criteria of a maximum number of iterations, PSO algorithm is unable to reach an equivalent depth of fitness values.

6.2. Damage case D_2

In the second case, two positions of double cracks depth will be analyzed as a complex problem to test the robustness of PSO-YUKI. The results are summarized in **Figure 8**. The results show that PSO is less effective compared to PSO-YUKI based on the convergence study. Fitness and estimated double cracks depth values of case 2 in 1, 15, 30, 50, 70, 85, and 100 iterations are presented in Table 9.

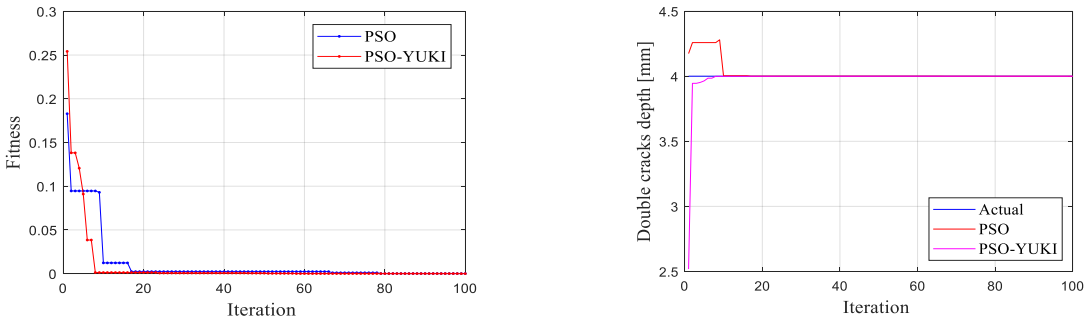

Test 1

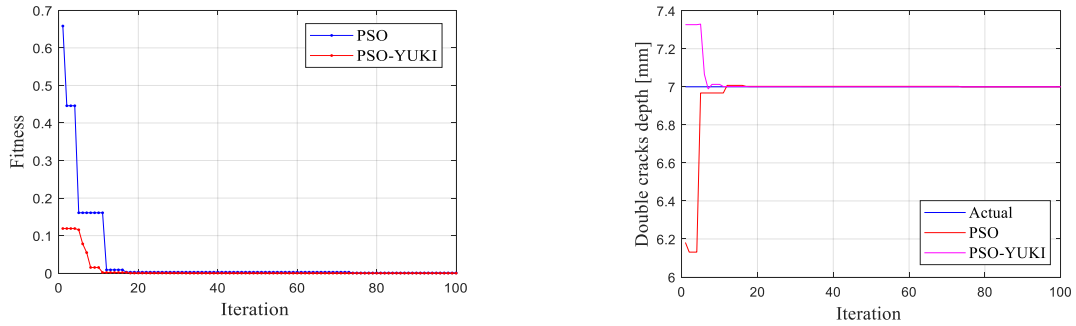

Test 2

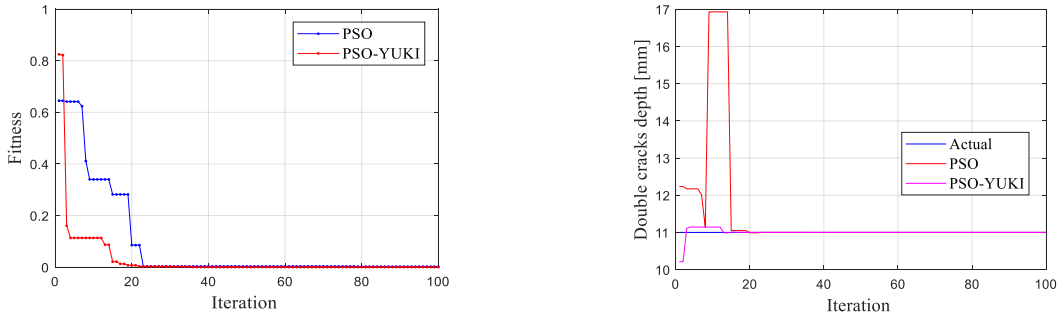

Test 3

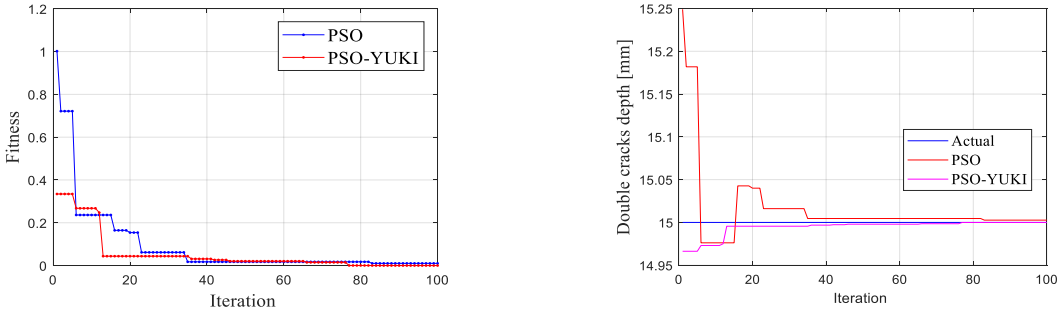

Test 4

Figure 8. PSO-RBF and PSO-YUKI-RBF performance for damage case D_2, predicting double cracks depth for 4 mm, 7 mm, 11 mm, and 15 mm.

Crack depth	Optimization techniques	Number of iteration	Fitness	Estimated crack depth
4	PSO	1	0.18291	4.17412
	YUKI-PSO		0.25418	2.51848
	PSO	15	0.01230	4.00374
	YUKI-PSO		0.00129	3.99949
	PSO	30	0.00235	4.00071
	YUKI-PSO		0.00074	3.99971
	PSO	50	0.00235	4.00071
	YUKI-PSO		0.00055	3.99978
	PSO	70	0.00105	4.00032
	YUKI-PSO		0.00008	4.00002
	PSO	85	0.00012	3.99995
	YUKI-PSO		0.00008	4.00002
	PSO	100	0.00012	3.99995
	YUKI-PSO		0.00002	4.00001
7	PSO	1	0.65827	6.18138
	YUKI-PSO		0.11890	7.32648
	PSO	15	0.00887	7.00739
	YUKI-PSO		0.00184	7.00153
	PSO	30	0.00268	7.00223
	YUKI-PSO		0.00030	7.00025

	PSO	50	0.00268	7.00223
	YUKI-PSO		0.00000	7.00000
	PSO	70	0.00268	7.00223
	YUKI-PSO		0.00000	7.00000
	PSO	85	0.00063	6.99987
	YUKI-PSO		0.00000	7.00000
	PSO	100	0.00063	6.99987
	YUKI-PSO		0.00000	7.00000
11	PSO	1	0.64483	12.23479
	YUKI-PSO		0.82443	10.21097
	PSO	15	0.28167	11.05024
	YUKI-PSO		0.02115	11.00693
	PSO	30	0.00288	11.00094
	YUKI-PSO		0.00214	11.00070
	PSO	50	0.00288	11.00094
	YUKI-PSO		0.00009	11.00003
	PSO	70	0.00288	11.00094
	YUKI-PSO		0.00009	11.00003
	PSO	85	0.00204	11.00067
	YUKI-PSO		0.00007	11.00002
	PSO	100	0.00204	11.00067
	YUKI-PSO		0.00000	11.00000
15	PSO	1	1.00189	15.24901
	YUKI-PSO		0.33449	14.96631
	PSO	15	0.23638	14.97617
	YUKI-PSO		0.04377	14.99558
	PSO	30	0.06167	15.01610
	YUKI-PSO		0.04377	14.99558
	PSO	50	0.01749	15.00458
	YUKI-PSO		0.02048	14.99793
	PSO	70	0.01749	15.00458
	YUKI-PSO		0.01495	14.99849
	PSO	85	0.01026	15.00269
	YUKI-PSO		0.00018	14.99998
	PSO	100	0.01026	15.00269
	YUKI-PSO		0.00018	14.99998

Table 9. Fitness and estimated double cracks depth values of case 2 in 1, 15, 30, 50, 70, 85, and 100 iterations

As seen in Table 9, the best analysis is boldfaced which is mostly provided by PSO-YUKI based on estimated crack depth and fitness. Although both algorithms reach a very close crack identity to the true one, in a relatively equivalent number of iterations, the suggested algorithm keeps making progress in a constant manner, while the classical algorithm stagnates. Reaching higher accuracy at the end of the search.

6.3. Damage case D_3

In the third case, three positions of double crack depth will be analysed as a more complex problem to test the robustness of PSO-YUKI. These results show that PSO-YUKI can accurately predict the crack depth in this damage case and is better than PSO alone. Results are summarized in **Figure 9**. Fitness and estimated double cracks depth values of case 2 in 1, 15, 30, 50, 70, 85, and 100 iterations are presented in Table 10**.**

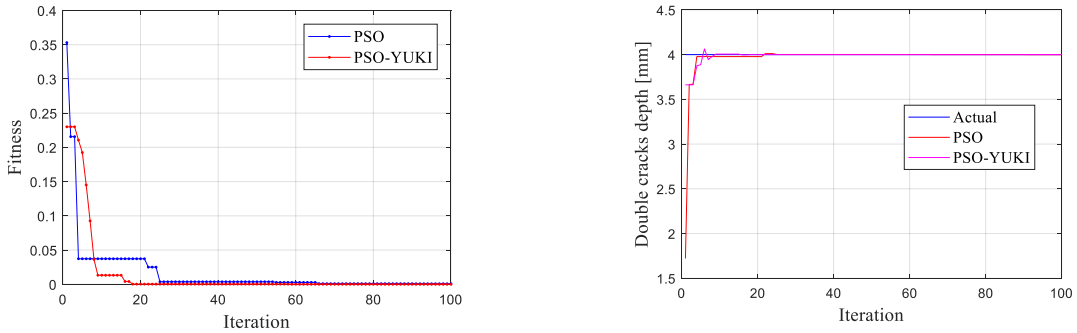

Test 1

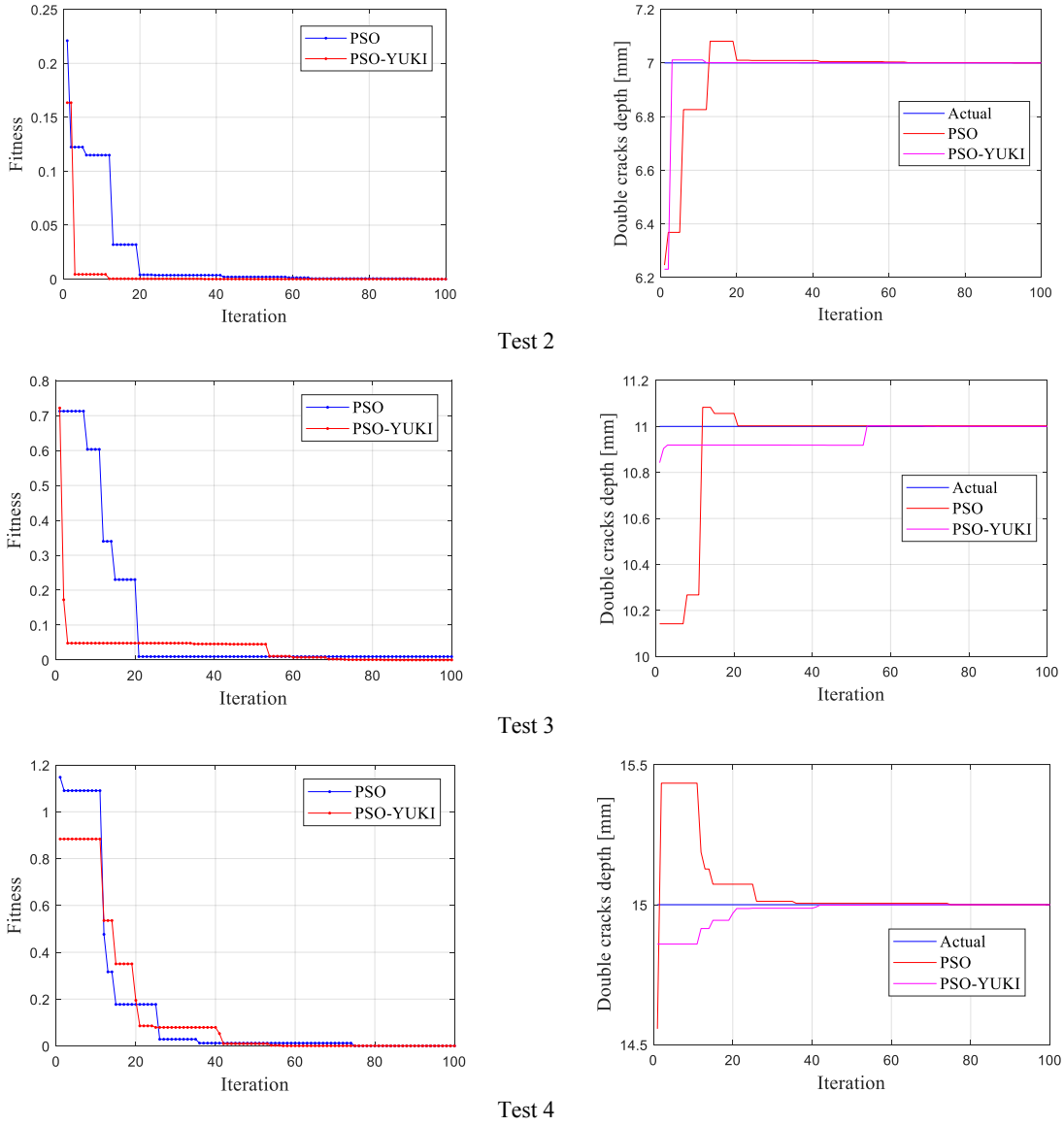

Figure 9. PSO-RBF and PSO-YUKI-RBF performance for damage case D_3, predicting double cracks depth for 4 mm, 7 mm, 11 mm, and 15 mm.

Crack depth	Optimization techniques	Number of iteration	Fitness	Estimated crack depth
4	PSO	1	0.35302	1.72110
	YUKI-PSO		0.23006	3.66197
	PSO	15	0.03730	3.97799
	YUKI-PSO		0.01322	4.00580
	PSO	30	0.00368	4.00161
	YUKI-PSO		0.00026	3.99985
	PSO	50	0.00368	4.00161
	YUKI-PSO		0.00026	3.99985
	PSO	70	0.00092	4.00040
	YUKI-PSO		0.00005	4.00002
	PSO	85	0.00092	4.00040
	YUKI-PSO		0.00000	4.00000
	PSO	100	0.00080	3.99953
	YUKI-PSO		0.00000	4.00000
7	PSO	1	0.22102	6.24637
	YUKI-PSO		0.16355	6.23105
	PSO	15	0.03199	7.08087
	YUKI-PSO		0.00034	7.00084
	PSO	30	0.00365	7.00907

	YUKI-PSO		0.00034	7.00084
	PSO	50	0.00202	7.00501
	YUKI-PSO		0.00002	7.00006
	PSO	70	0.00049	7.00122
	YUKI-PSO		0.00002	7.00004
	PSO	85	0.00041	7.00101
	YUKI-PSO		0.00002	7.00004
	PSO	100	0.00004	7.00011
	YUKI-PSO		0.00002	7.00004
11	PSO	1	0.71283	10.14210
	YUKI-PSO		0.72187	10.84243
	PSO	15	0.23031	11.05634
	YUKI-PSO		0.04817	10.91882
	PSO	30	0.00961	11.00236
	YUKI-PSO		0.04817	10.91882
	PSO	50	0.00961	11.00236
	YUKI-PSO		0.04523	10.91816
	PSO	70	0.00961	11.00236
	YUKI-PSO		0.00246	11.00060
	PSO	85	0.00961	11.00236
	YUKI-PSO		0.00023	11.00006
	PSO	100	0.00961	11.00236
	YUKI-PSO		0.00005	11.00001
15	PSO	1	1.14751	14.55633
	YUKI-PSO		0.88384	14.85929
	PSO	15	0.17739	15.07326
	YUKI-PSO		0.35046	14.94424
	PSO	30	0.02854	15.01210
	YUKI-PSO		0.07905	14.98743
	PSO	50	0.01194	15.00508
	YUKI-PSO		0.00943	14.99850
	PSO	70	0.01194	15.00508
	YUKI-PSO		0.00037	14.99994
	PSO	85	0.00009	15.00004
	YUKI-PSO		0.00009	14.99999
	PSO	100	0.00009	15.00004
	YUKI-PSO		0.00009	14.99999

Table 10. Fitness and estimated double cracks depth values of case 3 in 1, 15, 30, 50, 70, 85, and 100 iterations.

In Table 10, the best results are boldfaced which are mostly found by PSO-YUKI based on estimated crack depth and fitness in different iterations. The performance advantage of PSO-YUKI is clear in all examples. Indicating that the search strategy of forced focus can be an interesting idea to investigate further.

7. Experimental cracked beams

An experimental dynamic test was conducted on CFRP laminate specimens with the same double cracks position using three cases mentioned in Figure 3 **(**D_1, D_2, and D_3**)**. The experimental setup of the cracked beam is presented in Figure 10. The strike hummer, the accelerometer, and the real double crack positions of each scenario **(**D_1, D_2, and D_3**)** are shown in Figure 11.

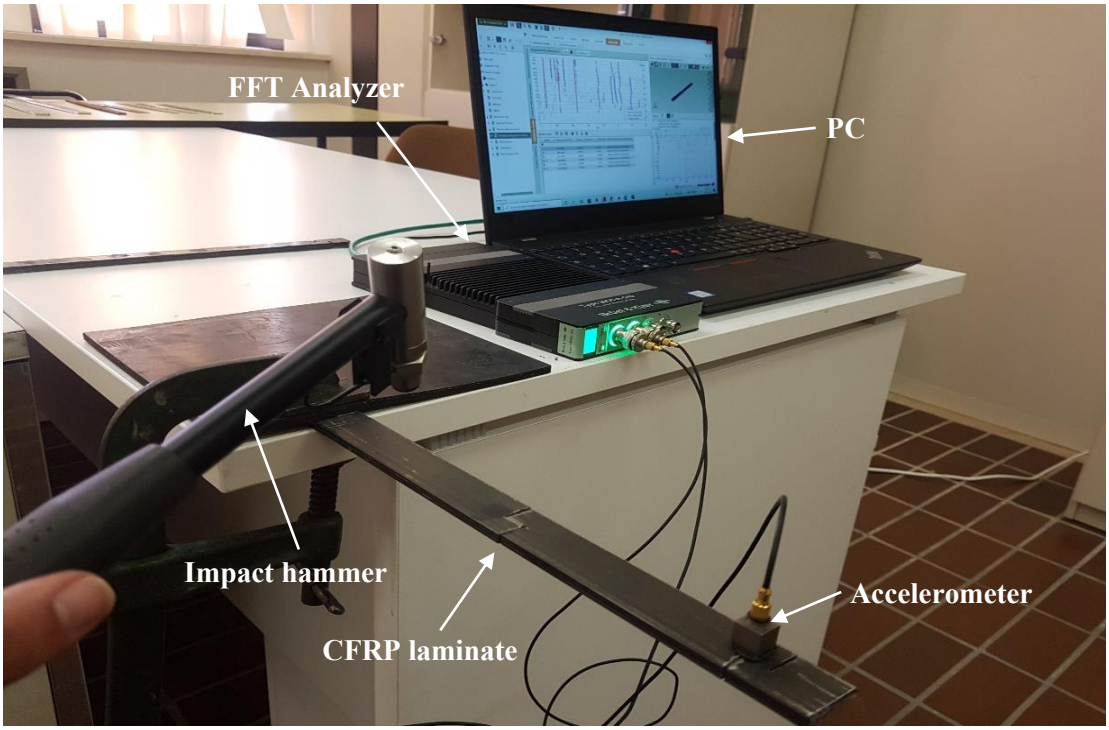

Figure 10. Operating mode for cracked beam modal analysis

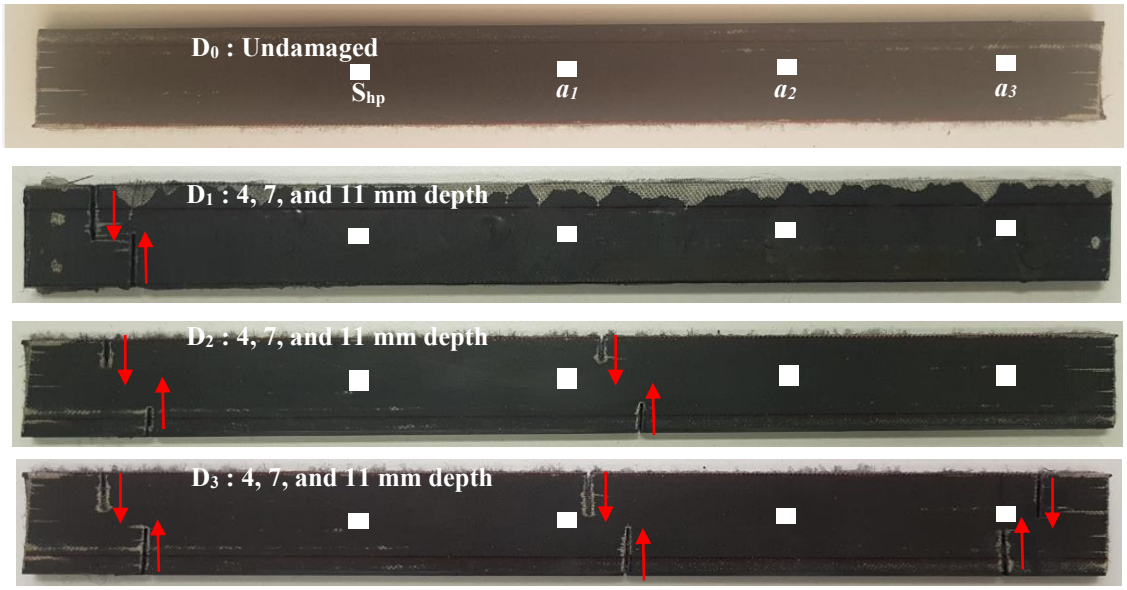

Figure 11. Applied double crack in three cases D_1, D_2, and D_3

The experimental envelope of Frequency Response Function (FRF) with measures of vibration recorded by the accelerometer for damaged beam model D_3 with 4, 7, and 11 mm crack depths are presented in Figure 12-13, respectively. In Table 11, the experimental and numerical frequencies values are shown for cracked beams based on three cases.

Crack depth (mm)		D_1			D_2			D_3		
		Mode 1	**Mode 2**	**Mode 3**	***Mode 1***	***Mode 2***	***Mode 3***	**Mode 1**	**Mode 2**	**Mode 3**
4	**Exp**	45.50	109.00	229.05	47.50	112.00	231.00	46.11	110.20	229.50
	Num	41.127	116.24	228.33	41.374	115.87	228.88	41.578	116.79	229.16
7	**Exp**	45.05	108.59	227.68	45.11	110.01	226.88	43.28	109.15	224.45
	Num	40.652	115.10	225.16	40 802	115.61	225.36	40.837	115.56	226.67
11	**Exp**	44.44	107.50	226.90	44.00	105.50	225.04	39.40	98.50	208.00
	Num	40.217	115.56	227.61	38 876	114.46	219.90	38.884	114.72	220.9

Table 11. Experimental frequency values for damaged CFRP laminate *D_1, D_2, and D_3*

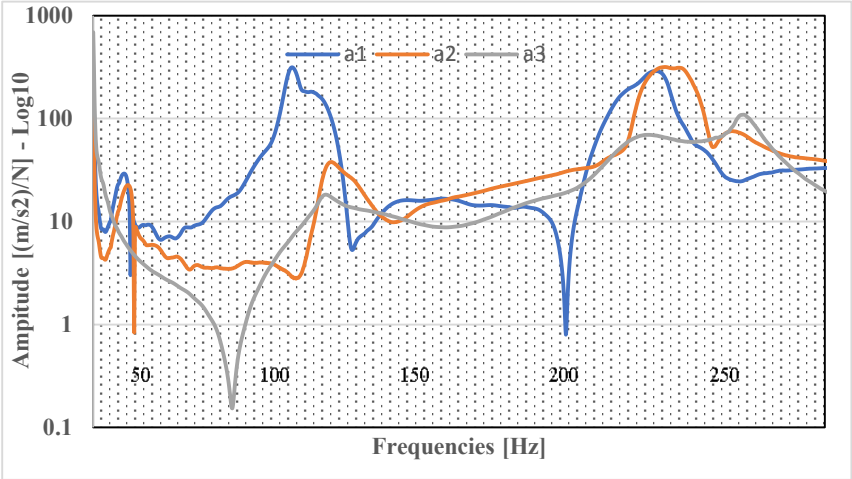

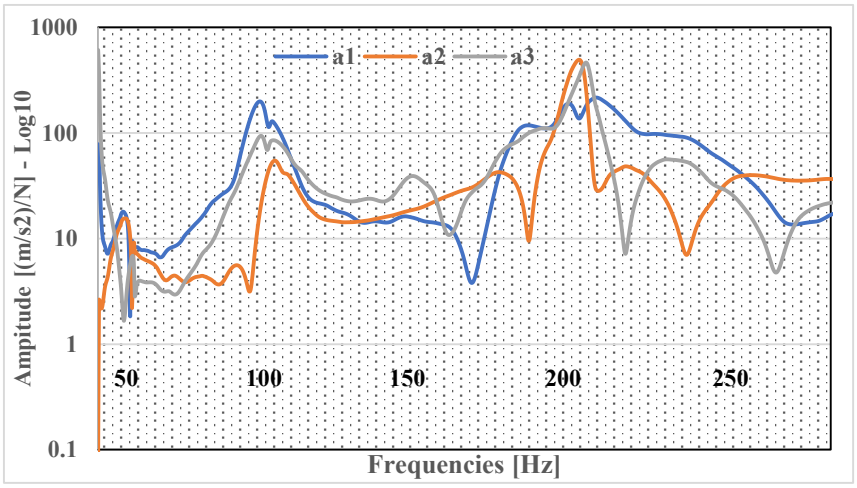

(b)

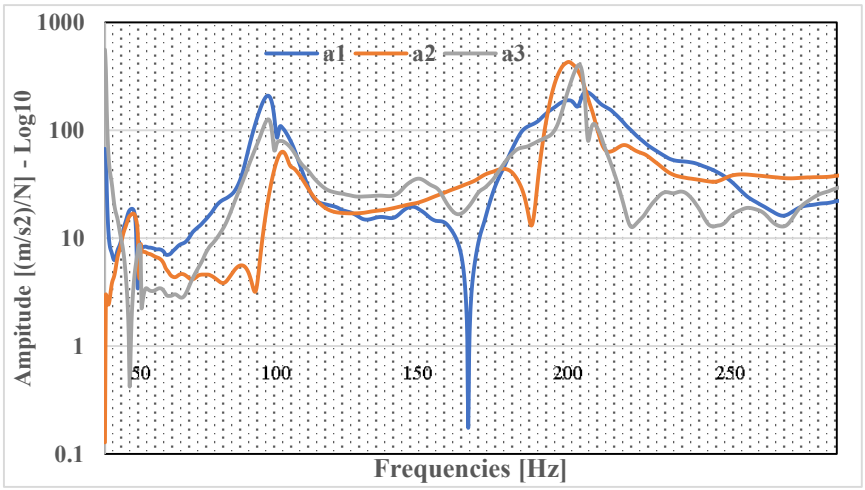

(C)

Figure 12. Experimental envelope of FRF diagrams for damaged CFRP laminate D_3 with crack depth 4 mm (a), 7 mm (b), and 11 mm (c) at accelerometer position a_1, a_2, and a_3

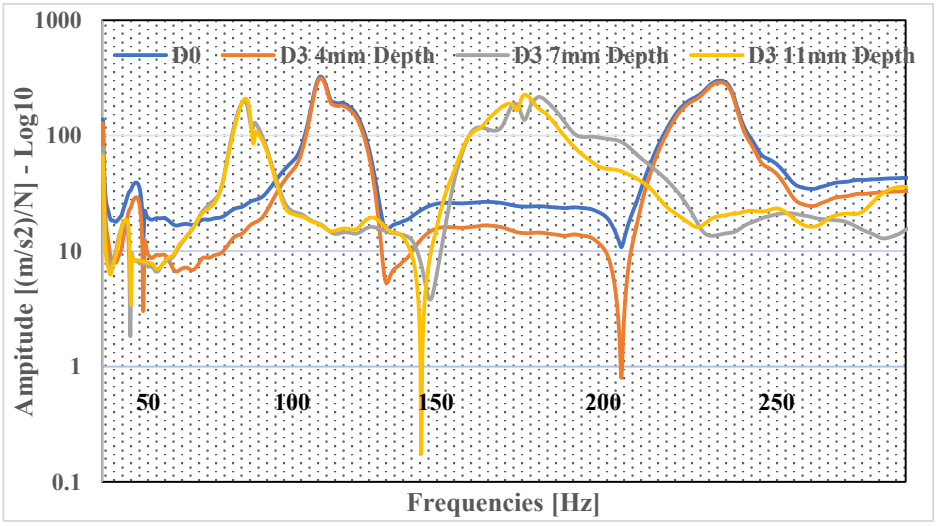

(a)

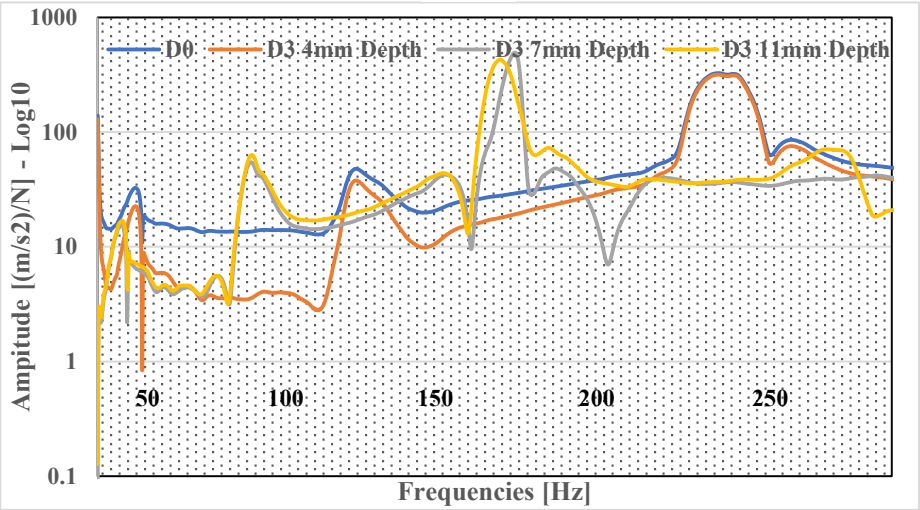

(b)

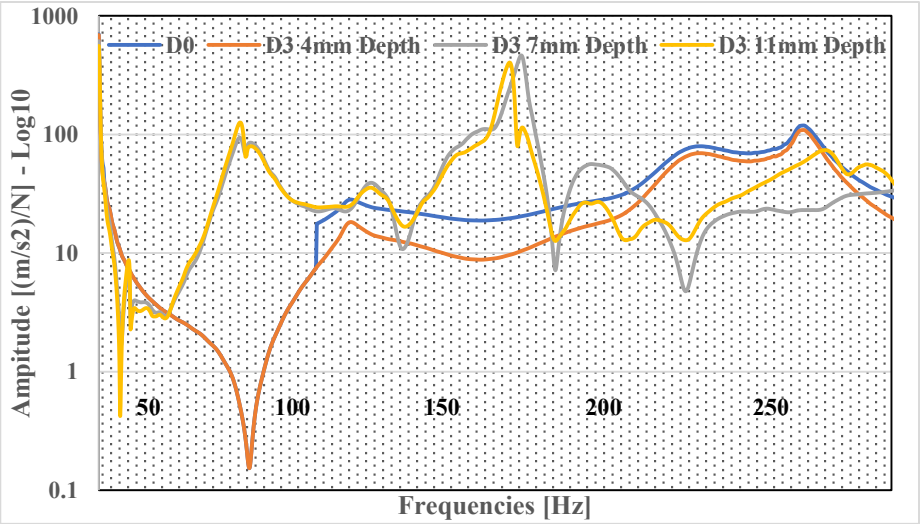

(C)

Figure 13. Comparison of envelopes of FRFs for undamaged and damaged CFRP laminates D_3 with double crack depth 4 mm, 7 mm, and 11 mm at accelerometer position a_1 (a), a_2 (b), and a_3 (c).

7.1 Results and discussions

In this section, to predict double crack depth considering D_1, D_2, and D_3 damage cases, the data collected from the experimental are mixed with numerical to prepare enough data that can be ready for prediction using RBF combined with PSO and PSO-YUKI after performing FEM. The provided results for each scenario in all cases are presented in **Figure 14**. The obtained results for each test show that the double crack depth have been found using both algorithms, however, the PSO-YUKI requires a less number of iterations to reach the correct results comparing to PSO. Furthermore, both algorithms present similar performance in terms of computation time, with PSO-YUKI slightly faster.

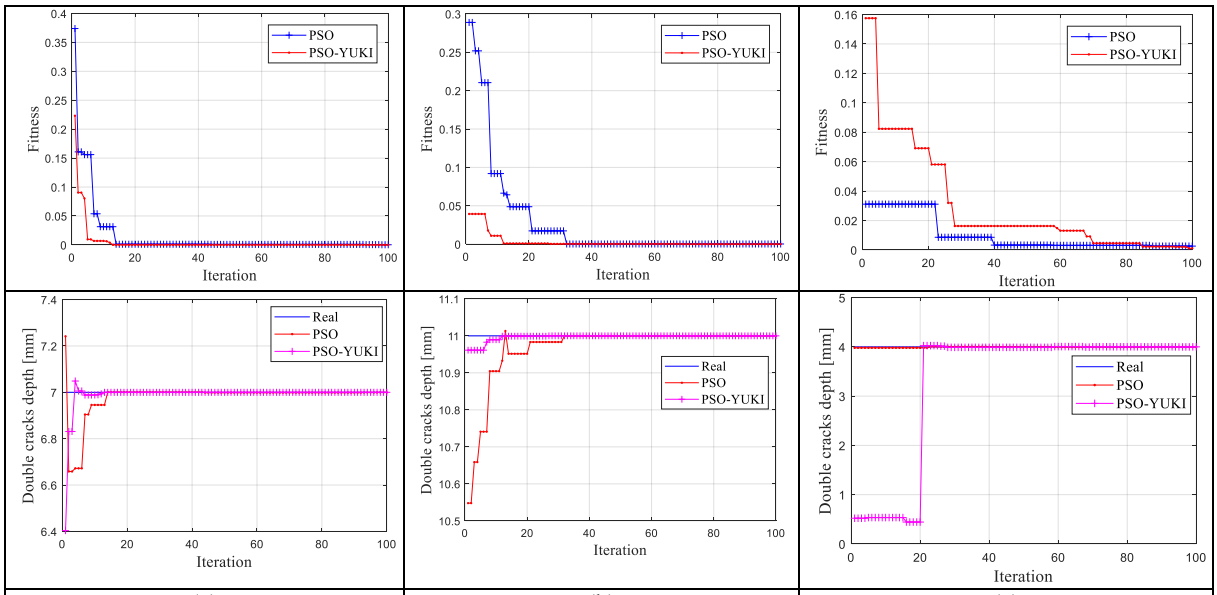

Figure 14. PSO and PSO-YUKI for experimental data, predicted double cracks depth for D_1 (a), D_2 (b), and D_3 (c).

8. Conclusion

In this paper, a computational intelligence approach based on PSO-YUKI hybrid intelligence has been created for damage prediction using a finite element model to build the databased into RBF as inverse problem analysis, considering diverse damage scenarios with increased crack depth. As the basis for the model, RBF is used, while PSO-YUKI is also used to improve the search for a better model, i.e. to find weight configurations allowing the model to converge to optimal values. The method is based on frequency input data and crack depth as output data. To evaluate the accuracy of the novel technique, experimental modal analysis was utilized to collect data for PSO-YUKI, and a comparison with PSO was made.

The expected output appears to be fairly close to the predicted results. The PSO-YUKI required a less number of iterations to get the optimal results compared to PSO, where the required number of iterations was greater. However, both approaches present a computational time somewhat similar, PSO-YUKI was slightly faster by a few seconds. The PSO-YUKI's accurate results prove that it is a reliable way for obtaining the required results, which, in turn, allows a crack to be identified with the lowest number of errors and iterations

References

1. Avci, O., et al., *A review of vibration-based damage detection in civil structures: From traditional methods to Machine Learning and Deep Learning applications.* Mechanical systems and signal processing, 2021. **147**: p. 107077.
2. Amezquita-Sanchez, J.P. and H. Adeli, *Signal processing techniques for vibration-based health monitoring of smart structures.* Archives of Computational Methods in Engineering, 2016. **23**(1): p. 1-15.
3. Chesné, S. and A. Deraemaeker, *Damage localization using transmissibility functions: A critical review.* Mechanical systems and signal processing, 2013. **38**(2): p. 569-584.
4. Meruane, V. and W. Heylen, *An hybrid real genetic algorithm to detect structural damage using modal properties.* Mechanical systems and signal processing, 2011. **25**(5): p. 1559-1573.

5. Khatir, S., et al., *Damage identification in steel plate using FRF and inverse analysis.* FRATTURA ED INTEGRITA STRUTTURALE-FRACTURE AND STRUCTURAL INTEGRITY, 2021. **58**: p. 416-433.
6. Lopes, H., J. Ribeiro, and J. Araújo dos Santos, *Interferometric techniques in structural damage identification.* Shock and Vibration, 2012. **19**(5): p. 835-844.
7. Capozucca, R., *Vibration of CFRP cantilever beam with damage.* Composite Structures, 2014. **116**: p. 211-222.
8. Viglietti, A., E. Zappino, and E. Carrera, *Free vibration analysis of locally damaged aerospace tapered composite structures using component-wise models.* Composite Structures, 2018. **192**: p. 38-51.
9. Carrera, E., A. Pagani, and M. Petrolo, *Free vibrations of damaged aircraft structures by component-wise analysis.* AIAA Journal, 2016. **54**(10): p. 3091-3106.
10. Pagani, A., M. Enea, and E. Carrera, *Component-wise damage detection by neural networks and refined FEs training.* Journal of Sound and Vibration, 2021. **509**: p. 116255.
11. Carrera, E. and A. Pagani, *Free vibration analysis of civil engineering structures by component-wise models.* Journal of Sound and Vibration, 2014. **333**(19): p. 4597-4620.
12. Hassan, N.M. and R. Batra, *Modeling damage in polymeric composites.* Composites Part B: Engineering, 2008. **39**(1): p. 66-82.
13. Capozucca, R., *A reflection on the application of vibration tests for the assessment of cracking in PRC/RC beams.* Engineering structures, 2013. **48**: p. 508-518.
14. Capozucca, R. and B. Bonci, *Notched CFRP laminates under vibration.* Composite Structures, 2015. **122**: p. 367-375.
15. Magagnini, E. and S. Khatir, *Effect of Damage by Notches in the Vibration Response of Homogeneous and Heterogeneous Beam Models*, in *Structural Health Monitoring and Engineering Structures*. 2021, Springer. p. 187-197.
16. Slimani, M., et al., *Experimental sensitivity analysis of sensor placement based on virtual springs and damage quantification in CFRP composite.* Journal of Materials and Engineering Structures «JMES», 2022. **9**(2): p. 207-220.
17. Behtani, A., et al., *Residual Force Method for damage identification in a laminated composite plate with different boundary conditions.* Frattura ed Integrità Strutturale, 2022. **16**(59): p. 35-48.
18. Pham, D.C. and X. Sun, *Experimental and computational studies on progressive failure analysis of notched cross-ply CFRP composite.* International Journal of Computational Materials Science and Engineering, 2012. **1**(03): p. 1250023.
19. Maa, R.-H. and J.-H. Cheng, *A CDM-based failure model for predicting strength of notched composite laminates.* Composites Part B: Engineering, 2002. **33**(6): p. 479-489.
20. Batra, R. and M. Lear, *Simulation of brittle and ductile fracture in an impact loaded prenotched plate.* International Journal of Fracture, 2004. **126**(2): p. 179-203.
21. Nakai, A., et al., *Mechanical properties and micro-fracture behaviors of flat braided composites with a circular hole.* Composite structures, 2001. **52**(3-4): p. 315-322.
22. Arora, S. and S. Singh, *Butterfly optimization algorithm: a novel approach for global optimization.* Soft Computing, 2019. **23**(3): p. 715-734.
23. Arora, S. and S. Singh, *An improved butterfly optimization algorithm with chaos.* Journal of Intelligent & Fuzzy Systems, 2017. **32**(1): p. 1079-1088.
24. Mukhopadhyay, T., et al., *Structural damage identification using response surface-based multi-objective optimization: a comparative study.* Arabian Journal for Science and Engineering, 2015. **40**(4): p. 1027-1044.
25. Xiang, J. and M. Liang, *A two-step approach to multi-damage detection for plate structures.* Engineering Fracture Mechanics, 2012. **91**: p. 73-86.
26. Benaissa, B., et al., *Crack identification using model reduction based on proper orthogonal decomposition coupled with radial basis functions.* Structural and Multidisciplinary Optimization, 2016. **54**(2): p. 265-274.

27. Althobiani, F., et al., *A hybrid PSO and Grey Wolf optimization algorithm for static and dynamic Crack identification.* Theoretical and Applied Fracture Mechanics, 2021: p. 103213.
28. Benaissa, B., et al. *Application of proper orthogonal decomposition and radial basis functions for crack size estimation using particle swarm optimization*. in *Journal of Physics: Conference Series*. 2017. IOP Publishing.
29. Khatir, S., et al. *Crack identification using eXtended IsoGeometric analysis and particle swarm optimization*. in *Fracture, fatigue and wear*. 2018. Springer.
30. Xiang, J., et al., *Crack detection in a shaft by combination of wavelet-based elements and genetic algorithm.* International journal of solids and structures, 2008. **45**(17): p. 4782-4795.
31. Samir, K., et al. *Genetic algorithm based objective functions comparative study for damage detection and localization in beam structures*. in *Journal of Physics: Conference Series*. 2015. IOP Publishing.
32. BENAISSA, B., I. BELAIDI, and A. HAMRANI, *IDENTIFYING DEFECT SIZE IN TWO DIMENSIONAL PLATES BASED ON BOUNDARY MEASUREMENTS USING REDUCED MODEL AND GENETIC ALGORITHM.* Journal of Sciences & Technology, 2017. **2**(1).
33. Jena, P.K. and D.R. Parhi, *A modified particle swarm optimization technique for crack detection in cantilever beams.* Arabian Journal for Science and Engineering, 2015. **40**(11): p. 3263-3272.
34. Khatir, S., et al. *Damage Identification in Frame Structure Based on Inverse Analysis*. in *Proceedings of the 2nd International Conference on Structural Damage Modelling and Assessment*. 2022. Springer.
35. Zare Hosseinzadeh, A., G. Ghodrati Amiri, and K.-Y. Koo, *Optimization-based method for structural damage localization and quantification by means of static displacements computed by flexibility matrix.* Engineering Optimization, 2016. **48**(4): p. 543-561.
36. Samir, K., et al., *Damage detection in CFRP composite beams based on vibration analysis using proper orthogonal decomposition method with radial basis functions and cuckoo search algorithm.* Composite Structures, 2018. **187**: p. 344-353.
37. Livani, M., N. Khaji, and P. Zakian, *Identification of multiple flaws in 2D structures using dynamic extended spectral finite element method with a universally enhanced meta-heuristic optimizer.* Structural and multidisciplinary optimization, 2018. **57**(2): p. 605-623.
38. Moezi, S.A., E. Zakeri, and A. Zare, *A generally modified cuckoo optimization algorithm for crack detection in cantilever Euler-Bernoulli beams.* Precision Engineering, 2018. **52**: p. 227-241.
39. Zhou, H., et al. *Structural identification using improved butterfly optimization algorithm with adaptive sampling test and search space reduction method*. in *Structures*. 2021. Elsevier.
40. Benaissa, B., et al., *YUKI algorithm and POD-RBF for Elastostatic and dynamic crack identification.* Journal of Computational Science, 2021: p. 101451.
41. Shirazi, M.I., et al., *Damage assessment in laminated composite plates using Modal Strain Energy and YUKI-ANN algorithm.* Composite Structures, 2022: p. 116272.
42. Bandara, R.P., T.H. Chan, and D.P. Thambiratnam, *Structural damage detection method using frequency response functions.* Structural Health Monitoring, 2014. **13**(4): p. 418-429.
43. Gomes, G.F., et al., *Optimized damage identification in CFRP plates by reduced mode shapes and GA-ANN methods.* Engineering Structures, 2019. **181**: p. 111-123.
44. Seguini, M., et al., *Crack prediction in pipeline using ANN-PSO based on numerical and experimental modal analysis.* Smart Structures and Systems, 2021. **27**(3): p. 507-523.
45. Khatir, S., et al., *An improved Artificial Neural Network using Arithmetic Optimization Algorithm for damage assessment in FGM composite plates.* Composite Structures, 2021. **273**: p. 114287.
46. Luo, C., et al., *EMCS-SVR: Hybrid efficient and accurate enhanced simulation approach coupled with adaptive SVR for structural reliability analysis.* Computer Methods in Applied Mechanics and Engineering, 2022. **400**: p. 115499.

47. Luo, C., et al., *Hybrid enhanced Monte Carlo simulation coupled with advanced machine learning approach for accurate and efficient structural reliability analysis.* Computer Methods in Applied Mechanics and Engineering, 2022. **388**: p. 114218.
48. Meng, D., et al., *Multidisciplinary design optimization of engineering systems under uncertainty: a review.* International Journal of Structural Integrity, 2022(ahead-of-print).
49. Meng, D., et al., *Structural reliability analysis and uncertainties-based collaborative design and optimization of turbine blades using surrogate model.* Fatigue & Fracture of Engineering Materials & Structures, 2019. **42**(6): p. 1219-1227.
50. Zhu, S.-P., et al., *Computational-experimental approaches for fatigue reliability assessment of turbine bladed disks.* International Journal of Mechanical Sciences, 2018. **142**: p. 502-517.
51. Kennedy, J. and R. Eberhart. *Particle swarm optimization*. in *Proceedings of ICNN'95-international conference on neural networks*. 1995. IEEE.
52. Buljak, V. and G. Maier, *Proper orthogonal decomposition and radial basis functions in material characterization based on instrumented indentation.* Engineering Structures, 2011. **33**(2): p. 492-501.
53. Arora, Y., A. Singhal, and A. Bansal, *A study of applications of RBF network.* International Journal of Computer Applications, 2014. **94**(2).
54. Sharma, O. *Deep challenges associated with deep learning*. in *2019 international conference on machine learning, big data, cloud and parallel computing (COMITCon)*. 2019. IEEE.
55. Suganthan, P.N., et al., *Problem definitions and evaluation criteria for the CEC 2005 special session on real-parameter optimization.* KanGAL report, 2005. **2005005**(2005): p. 2005.